# Interpreting Moving Mesh Methods and Transformation Techniques from Various Applications in Terms of the Mass Transport Problem

by

Mohamed H. Mahmoud Sulman

B. Sc. Al-Neelain University, 1993

M. Sc. Tsinghua University, 2000

A THESIS SUBMITTED IN PARTIAL FULFILLMENT
OF THE REQUIREMENTS FOR THE DEGREE OF
MASTER OF SCIENCE
IN THE DEPARTMENT
OF
MATHEMATICS



SIMON FRASER UNIVERSITY

October 2003

# APPROVAL

**Name:** Mohamed H. Mahmoud Sulman

**Degree:** Master of Science

**Title of thesis:** Interpreting Moving Mesh Methods and Transformation Techniques from Various Applications in Terms of the Mass Transport Problem

**Examining Committee:** Dr. Ralf Wittenberg
Chair

Dr. Robert Russell
Senior Supervisor

Dr. Steve Ruuth
Supervisor

Dr. Mary Catherine Kropinski
Supervisor

Dr. John Stockie
Internal/External Examiner

**Date Approved:** October 30, 2003

## PARTIAL COPYRIGHT LICENCE



**Title of Thesis/Project/Extended Essay**

Interpreting Moving Mesh Methods and Transformation Techniques from Various Applications in terms of the Mass Transport Problem

**Author:**

(signature)

Mohamad Hamid Mahmoud Sulman

(name)

11/27/2003

(date)

# Contents

# List of Figures

# Abstract

Over the last twenty years, moving mesh methods have become a very useful tool for solving many partial differential equations (PDEs) numerically, in particular, PDEs having large solution variations such as boundary layers, shock waves, blow-up, and moving wave fronts. Various types of moving mesh methods have been developed to solve such problems. These methods generally use a non-uniform mesh with a fixed number of mesh points as time evolves. The points are concentrated in regions with steep solutions. In their recent paper, Cao, Huang and Russell introduce a moving mesh method based on specifying the Jacobian of the coordinate transformation, the geometric conservation law (GCL) and a curl condition. In this thesis, we study the relationship between the resulting GCL method and the Monge-Kantorovich mass transfer problem: a civil engineering problem first formulated by Monge in 1781. The transfer problem is concerned with finding the optimal path, in the sense of moving parcels of materials from one site to another one with minimal transportation cost. We also investigate the link between moving mesh theory and fluid dynamics, meteorology, computational anatomy and image registration by establishing a relationship between the coordinate transformations used in their formulations.

# Acknowledgments

I would like to sincerely thank my supervisor Dr. Robert D. Russell for his patience, guidance, encouragement and constant support, which made my studies here possible.

Special thanks go to Dr. Wentao Sun, for his suggestions in various parts of my thesis and for his help in writing the Fortran code.

Special thanks also go to Dr. Jinyun Yuan and my colleagues Benjamin Ong and Colin Macdonald, for their constructive comments.

I would also like to thank Dr. Weiming Cao, for making the GCL code available.

My sincere gratitude goes to the staff and faculty of Mathematics department at Simon Fraser University, for their cooperation and constant support throughout my studies here.

Last but not least, I would like to acknowledge the support of my wife Maalim Eltigani, who has helped me in many ways over the last several years.

# Chapter 1

# Mathematical Background

Transformation techniques have been used in many different areas of mathematics. For example, transformation techniques have been used to describe the Lagrangian method for solving computational fluid dynamics problems, the Monge-Kantorovich mass transfer problem and moving mesh methods for mesh adaption.

In this chapter we review some basic definitions and theorems from calculus and vector analysis that we encounter in some parts of the thesis.

## 1.1 Vector Fields

Points in a plane can be identified by using a two-dimensional Cartesian co-ordinate system. A plane together with the Cartesian co-ordinate system is called the xy-plane and is denoted by $\mathbb{R}^2$,

$$\mathbb{R}^2 = \{(x, y) \mid x \in \mathbb{R}, \ y \in \mathbb{R}\},$$

where $\mathbb{R}$ is the set of all real numbers. The set

$$\mathbb{R}^3 = \{(x, y, z) \mid x, \ y, \ z \in \mathbb{R}\}$$

describes all the points in three-dimensional space. Similarly, points in $n$-dimensional space are defined as

$$\mathbb{R}^n = \{(x_1, x_2, \ldots, x_n) \mid x_i \in \mathbb{R}\}. \tag{1.1}$$

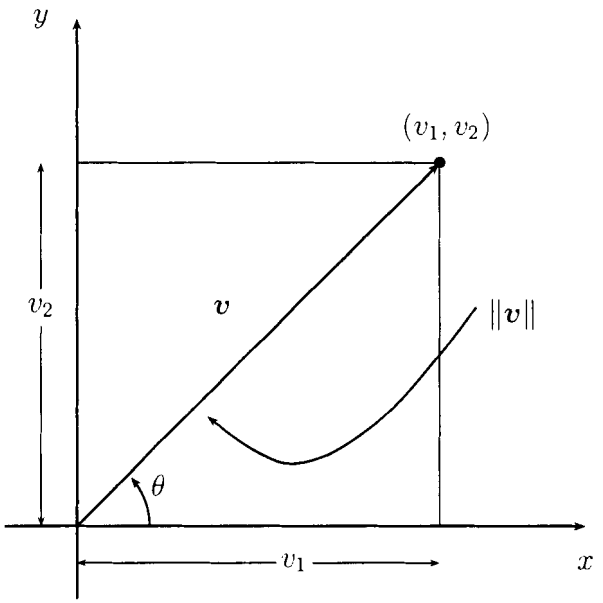


Figure 1.1: Representation of a vector in a plane.

**Definition 1.1.** A vector is a quantity characterized by both magnitude and direction. A vector in $\mathbb{R}^n$ is an ordered $n$-tuple $\boldsymbol{v} = (v_1, v_2, \ldots, v_n)$ of real numbers. In particular, a vector in $\mathbb{R}^2$ is an ordered pair $\boldsymbol{v} = (v_1, v_2)$, and a vector in $\mathbb{R}^3$ is an ordered triple $\boldsymbol{v} = (v_1, v_2, v_3)$. The real numbers are called the components or the coordinates of $\boldsymbol{v}$. The length of a vector in $\mathbb{R}^2$ is defined as (see figure 1.1)

$$\|\boldsymbol{v}\| = \sqrt{v_1^2 + v_2^2}, \tag{1.2}$$

and for $\boldsymbol{v} = (v_1, v_2, \ldots, v_n) \in \mathbb{R}^n$.

$$\|\boldsymbol{v}\| = \sqrt{v_1^2 + v_2^2 + \cdots + v_n^2}. \tag{1.3}$$

□

**Definition 1.2.** The dot product of two vectors $\boldsymbol{v} = (v_1, v_2, \ldots, v_n)$ and $\boldsymbol{w} = (w_1, w_2, \ldots, w_n) \in \mathbb{R}^n$, $n \geq 2$ is the real number $\boldsymbol{v} \cdot \boldsymbol{w}$ defined by

$$\boldsymbol{v} \cdot \boldsymbol{w} = v_1 w_1 + v_2 w_2 + \cdots + v_n w_n. \tag{1.4}$$

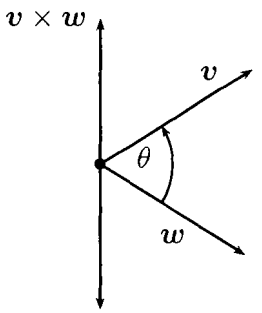


Figure 1.2: Geometric representation of vector product.

An equivalent definition of the dot product of two vectors in $\mathbb{R}^2$ or $\mathbb{R}^3$ is

$$\boldsymbol{v} \cdot \boldsymbol{w} = \|\boldsymbol{v}\|\|\boldsymbol{w}\| \cos\theta,$$

where $\theta$ is the angle between $\boldsymbol{v}$ and $\boldsymbol{w}$. This definition implies

$$\boldsymbol{v} \cdot \boldsymbol{w} = 0 \text{ if and only if } \boldsymbol{v} \text{ and } \boldsymbol{w} \text{ are orthogonal.}$$

□

**Definition 1.3.** The vector product of two vectors is an operation that assigns a vector to two given vectors. Unlike the dot product, it is defined only for vectors in $\mathbb{R}^3$. The vector product of two vectors $\boldsymbol{v} = v_1\mathbf{i} + v_2\mathbf{j} + v_3\mathbf{k}$ and $\boldsymbol{w} = w_1\mathbf{i} + w_2\mathbf{j} + w_3\mathbf{k}$ is the vector $\boldsymbol{v} \times \boldsymbol{w}$ defined as

$$\boldsymbol{v} \times \boldsymbol{w} = \begin{vmatrix} \mathbf{i} & \mathbf{j} & \mathbf{k} \\ v_1 & v_2 & v_3 \\ w_1 & w_2 & w_3 \end{vmatrix} = (v_2w_3 - v_3w_2)\mathbf{i} - (v_1w_3 - v_3w_1)\mathbf{j} + (v_1w_2 - v_2w_3)\mathbf{k}.$$

□

The direction of the vector $\boldsymbol{v} \times \boldsymbol{w}$ is determined by the right-hand rule (see figure 1.2).

In $\mathbb{R}^2$ and $\mathbb{R}^3$ an equivalent definition of the vector product of two vectors $\boldsymbol{v}$ and $\boldsymbol{w}$ is

$$\boldsymbol{v} \times \boldsymbol{w} = \|\boldsymbol{v}\|\|\boldsymbol{w}\| \sin\theta\, \hat{\mathbf{e}}, \tag{1.5}$$

where $\hat{\mathbf{e}}$ is a unit vector normal to both $\boldsymbol{v}$ and $\boldsymbol{w}$. (1.5) shows that non-zero vectors $\boldsymbol{v}$ and $\boldsymbol{w}$ are parallel if and only if $\boldsymbol{v} \times \boldsymbol{w} = \mathbf{0}$. The tangential velocity $\boldsymbol{v}$ of a body rotating with constant angular speed $w$ about a certain axis in space is defined as

$$\boldsymbol{v} = \boldsymbol{w} \times \mathbf{r},$$

where $\boldsymbol{w}$ is the angular velocity with magnitude $w$ and $\mathbf{r}$ is the position vector of the rotating body.

## 1.2 Calculus of Functions of Several Variables

In this section we introduce some definitions and theorems on functions of several variables.

**Definition 1.4.** A function whose domain is a subset of $\mathbb{R}^m$ and whose range is contained in $\mathbb{R}^n$ is called a real-valued function of m variables if $n = 1$, and a vector-valued function of m variables if $n > 1$. Real-valued functions are also called scalar-valued or just scalar functions.

□

**Definition 1.5.** A vector field on $\Omega \subseteq \mathbb{R}^m$ is a vector-valued function $\mathbf{F} : \Omega \longrightarrow \mathbb{R}^m$ defined on a subset $\Omega$ of $\mathbb{R}^m$.

□

Although the domain and the range of a vector field belong to the same set $\mathbb{R}^m$, we often visualize them in a different way: we can think of the elements of the domain as points, whereas we can view the elements of the range as vectors. For example, a vector field on $\mathbb{R}^3$ is a function that assigns a vector $\mathbf{F}(x, y, z)$ to every point $(x, y, z)$ in the three-dimensional space $\mathbb{R}^3$. This interpretation helps us graph a vector field :

its value $\mathbf{F}(x, y, z)$ at $(x, y, z)$ is represented as a vector $\mathbf{F}(x, y, z)$ whose initial point is $(x, y, z)$. Similarly, a vector field on $\mathbb{R}^2$ assigns the vector $\mathbf{F}(x, y) \in \mathbb{R}^2$ to each point $(x, y)$ in its domain.

There are some situations when it is more convenient to visualize a vector-valued function $\mathbf{F} : \Omega \subseteq \mathbb{R}^m \to \mathbb{R}^m$ as a mapping of points. This is a useful way of thinking about $\mathbf{F}$, for example, in the change of variables technique used for solving partial differential equations.

**Definition 1.6.** Consider a function $\boldsymbol{x} : [a, b] \to \mathbb{R}^3$ defined on an interval [a,b] of real numbers. The value $\boldsymbol{x}$ at $t \in [a, b]$ can be interpreted as a point $\boldsymbol{x}(t) = (x(t), y(t), z(t))$ in space; as $t$ changes from a to b, the values $\boldsymbol{x}(t)$ defines a curve in $\mathbb{R}^3$. Similarly a function $\boldsymbol{x} : [a, b] \to \mathbb{R}^2$ describes a curve in the $xy$-plane.

□

**Definition 1.7.** Let $\mathbf{F}(\boldsymbol{x})$ be a vector-valued function $\mathbf{F} : \Omega \subset \mathbb{R}^m \to \mathbb{R}^n$. We denote the $n \times m$ matrix of partial derivatives of the components $\mathbf{F}$ evaluated at $\boldsymbol{x}$ as

$$D\mathbf{F}(\boldsymbol{x}) = \begin{bmatrix} \frac{\partial F_1}{\partial x_1} & \frac{\partial F_1}{\partial x_2} & \cdots & \frac{\partial F_1}{\partial x_m} \\ \frac{\partial F_2}{\partial x_1} & \frac{\partial F_2}{\partial x_2} & \cdots & \frac{\partial F_2}{\partial x_m} \\ \vdots & \vdots & & \vdots \\ \frac{\partial F_n}{\partial x_1} & \frac{\partial F_n}{\partial x_2} & \cdots & \frac{\partial F_n}{\partial x_m} \end{bmatrix}, \tag{1.6}$$

provided that all partial derivatives exist at $\boldsymbol{x}$. If $F : \mathbb{R} \to \mathbb{R}$ then $DF(x)$ is $1 \times 1$ matrix and $DF(x)$ is the usual derivative $F'(x)$. Assume that $F(\boldsymbol{x}) : \Omega \subset \mathbb{R}^m \to \mathbb{R}$ is a real-valued function of m variables . Then $DF(\boldsymbol{x})^T$ is the $m \times 1$ matrix

$$DF(\boldsymbol{x})^T = \begin{bmatrix} \frac{\partial F}{\partial x_1} & \frac{\partial F}{\partial x_2} & \cdots & \frac{\partial F}{\partial x_m} \end{bmatrix}^T, \tag{1.7}$$

$DF(\boldsymbol{x})^T$ is called the gradient of $F$ at $\boldsymbol{x}$ and is denoted by $\nabla F(\boldsymbol{x})$.

□

**Definition 1.8.** A vector-valued function $\mathbf{F} : \Omega \subset \mathbb{R}^m \to \mathbb{R}^n$ defined on an open set $\Omega \subset \mathbb{R}^m$ is differentiable at a point $\boldsymbol{x}_0 \in \Omega$ if

1. all partial derivatives of the components $F_1, F_2, \ldots, F_n$ of $\mathbf{F}$ exist at $\boldsymbol{x}_0$, and

2. the matrix of partial derivatives $D\mathbf{F}(\boldsymbol{x}_0)$ of $\mathbf{F}$ at $\boldsymbol{x}_0$ satisfies

$$\lim_{\boldsymbol{x}\to\boldsymbol{x}_0} \frac{\| \mathbf{F}(\boldsymbol{x}) - \mathbf{F}(\boldsymbol{x}_0) - D\mathbf{F}(\boldsymbol{x}_0)(\boldsymbol{x}-\boldsymbol{x}_0) \|}{\| \boldsymbol{x}-\boldsymbol{x}_0 \|} = 0, \tag{1.8}$$

where $\| \cdot \|$ in the numerator denotes the length in $\mathbb{R}^n$, and $\| \cdot \|$ in the denominator is the length in $\mathbb{R}^m$.

□

If a vector-valued function $\mathbf{F}$ satisfies the conditions (1) and (2) of definition [1.8], the matrix defined in (1.6) is called the derivative of $\mathbf{F}$ at $\boldsymbol{x}_0$.

**Theorem 1.1.** Let $\mathbf{F} : \Omega \subset \mathbb{R}^m \to \mathbb{R}^n$ be a vector-valued function with components $F_1, F_2 \ldots F_n : \Omega \subset \mathbb{R}^m \to \mathbb{R}$. If all partial derivatives

$$\frac{\partial F_i}{\partial x_j}, \quad i = 1,\ 2, \ldots,\ n,\ j = 1,\ 2,\ \ldots\ , m,$$

are continuous at $\boldsymbol{x}_0$, then $\mathbf{F}$ is differentiable at $\boldsymbol{x}_0$.

□

**Definition 1.9.** A function whose partial derivatives exist and are continuous is said to be in the class of $C^1$ or smooth functions.

□

In the following we give some brief introduction to Monge-Ampere equations.

**Definition 1.10.** A Monge-Ampere equation is a second order partial differential equation of the form (see [46])

$$H\phi_{xx} + 2K\phi_{xy} + L\phi_{yy} + M + N(\phi_{xx}\phi_{yy} - \phi_{xy}^2) = 0, \tag{1.9}$$

where $H, K, L, M$, and $N$ are functions of $x, y, \phi, \phi_x$ and $\phi_y$.

Simplified Monge-Ampere equations arise in the form (see [47] and [48])

$$u_{xx}u_{yy} - u_{xy}^2 = f(x, y, u_x, u_y) \tag{1.10}$$

and

$$\begin{vmatrix} u_{x_1x_1} & u_{x_1x_2} & \dots & u_{x_1x_n} \\ u_{x_2x_1} & u_{x_2x_2} & \dots & u_{x_2x_n} \\ \vdots & \vdots & & \vdots \\ u_{x_nx_1} & u_{x_nx_2} & \dots & u_{x_nx_n} \end{vmatrix} = f(x, y, u, \nabla u) \tag{1.11}$$

□

The classical Monge-Ampere equation (1.10) has been the center of considerable interest in recent years because of its important role in various areas of applied mathematics. Also, Monge-Ampere type equations have applications in the areas of differential geometry, the calculus of variations, and several optimization problems, such as the Monge-Kantorovich mass transfer problem [1].

For future reference, we state the following Helmholtz decomposition theorem.

**Theorem 1.2.** Let $\Omega$ be a smooth bounded connected open set in $\mathbb{R}^n$. Then any vector field $\boldsymbol{v}$ with continuous first derivatives in $\Omega$ can be written uniquely as

$$\boldsymbol{v} = \mathbf{u} + \nabla\phi,$$

where $\phi$ is a smooth potential function, defined on $\Omega$ up to an additive constant, and $\mathbf{u}$ is a smooth divergence free vector field (i.e,$\nabla \cdot \mathbf{u} = 0$), parallel to the boundary of $\Omega$. Note that $\nabla\phi$ is irrotational since $\nabla \times \nabla\phi = \mathbf{0}$.

□

The Helmholtz decomposition theorem [44] is the simplest application of the Hodge decomposition theorem (see [42]). Brenier [3] shows that the Helmholtz decomposition is a linearization of the polar factorization of vector-valued functions.

# Chapter 2

# General Theory

In this chapter we introduce the ideas behind fluid dynamics, moving mesh methods, the mass transfer problem, semi-geostrophic equations and computational anatomy.

## 2.1 Fluid Dynamics

Fluid dynamics describes the motion of liquids and gases in response to applied forces.

Consider a fluid in an arbitrary volume $\Omega(t)$, moving with velocity $\boldsymbol{v}(\boldsymbol{x}, t)$. Then the fluid motion can be described by following the fluid particle path lines $\boldsymbol{x}(t)$ controlled by the equation

$$\frac{\mathrm{d}\boldsymbol{x}}{\mathrm{d}t} = \boldsymbol{v}(\boldsymbol{x}(t), t), \quad \boldsymbol{x}(0) = \boldsymbol{x}_0. \tag{2.1}$$

The above description of fluid motion is called the Lagrangian formulation.

The study of fluid motion provides us with the capability of understanding the transport of mass, momentum and energy. The equations of fluid dynamics are best described via conservation laws for mass, momentum, and energy. These conservation laws are given in terms of challenging nonlinear PDEs. For future reference, in this section we discuss the conservation laws for mass and momentum. In deriving the conservation laws, one frequently faces the problem of finding the time derivative of integrals such as

$$\frac{\mathrm{d}}{\mathrm{d}t} \int_{\Omega(t)} F(\boldsymbol{x}, t)\, d\boldsymbol{x}, \tag{2.2}$$

where the $F(\boldsymbol{x}, t)$ can be a scalar or vector-valued function, $\Omega(t)$ is either a fixed or a material volume (i.e., consists of the same fluid particles and whose bounding surface moves with the fluid). In one-dimensional space, we have Leibniz's rule

$$\frac{\mathrm{d}}{\mathrm{d}t}\int_a^b F(x,t)\,dx = \int_a^b \frac{\partial F}{\partial t}\,dx + F(b,t)\frac{\mathrm{d}b}{\mathrm{d}t} - F(a,t)\frac{\mathrm{d}a}{\mathrm{d}t} \tag{2.3}$$

to compute the integral (2.2). Generalizing Leibinz's rule, in two and three dimensions we write

$$\frac{\mathrm{d}}{\mathrm{d}t}\int_{\Omega(t)} F(\boldsymbol{x},t)\,d\boldsymbol{x} = \int_{\Omega(t)} \frac{\partial F}{\partial t}\,d\boldsymbol{x} + \int_{\partial\Omega(t)} F\boldsymbol{v}\cdot\mathbf{n}dS, \tag{2.4}$$

where $\boldsymbol{v}$ is the velocity of the boundary, which is equal to the fluid velocity when $\Omega(t)$ is a material volume and $\mathbf{n}$ is a unit vector normal to the surface of $\Omega(t)$. (2.4) is called *the Reynolds transport theorem.* Using the divergence theorem the transport equation (2.4) can be written equivalently as

$$\frac{\mathrm{d}}{\mathrm{d}t}\int_{\Omega(t)} F(\boldsymbol{x},t)\,d\boldsymbol{x} = \int_{\Omega(t)} \left[\frac{\partial F}{\partial t} + \nabla\cdot(F\boldsymbol{v})\right] d\boldsymbol{x}. \tag{2.5}$$

The conservation laws can be derived by using (2.5). Since $\Omega$ is an arbitrary test volume, then from the Reynolds transport theorem for $F = \rho$ (the fluid density) follows the conservation law for mass

$$\frac{\partial\rho}{\partial t} + \nabla\cdot(\rho\boldsymbol{v}) = 0, \tag{2.6}$$

which is sometimes called *the continuity equation.* If the fluid is incompressible, then the continuity equation reduces to

$$\nabla\cdot\boldsymbol{v} = 0. \tag{2.7}$$

To derive the equation for conservation of momentum, Newton's second law of mechanics can be written as

$$\frac{\mathrm{d}\boldsymbol{m}}{\mathrm{d}t} = \mathbf{f}, \tag{2.8}$$

where $\mathbf{f}$ is the total force acting on the fluid volume and $\boldsymbol{m}$ is the total momentum written as

$$\boldsymbol{m} = \int_{\Omega(t)} \rho\,\boldsymbol{v}\,d\boldsymbol{x}. \tag{2.9}$$

The total force $\mathbf{f}$ can be written as (see [45])

$$\mathbf{f} = \int_{\Omega(t)} (\mathbf{f}_1 + \mathbf{f}_2 + \mathbf{f}_3)\, d\boldsymbol{x}, \tag{2.10}$$

where $\mathbf{f}_1$ is internal pressure, $\mathbf{f}_2$ is the viscosity dissipation in the fluid, and $\mathbf{f}_3$ represents the external forces.

The momentum equation can be derived by using the Reynolds transport theorem (2.5). To this end, consider an incompressible fluid flow where $\rho$ = constant. For $F = \rho\boldsymbol{v}$ (momentum per unit mass), (2.5) gives

$$\frac{\partial \boldsymbol{v}}{\partial t} + \boldsymbol{v} \cdot \nabla \boldsymbol{v} = \frac{1}{\rho}(\mathbf{f}_1 + \mathbf{f}_2 + \mathbf{f}_3). \tag{2.11}$$

The conservation of momentum is described by (2.11). For an incompressible fluid flow, it is shown that (see [45])

$$\mathbf{f}_1 = -\nabla P, \quad \mathbf{f}_2 = \mu \nabla^2 \boldsymbol{v}, \tag{2.12}$$

where $P$ is the fluid pressure and $\mu$ is the viscosity of the fluid. Thus, for $\mathbf{f}_3 = \rho\mathbf{g}$ (only the gravity), the momentum equation (2.11) gives

$$\frac{\partial \boldsymbol{v}}{\partial t} + \boldsymbol{v} \cdot \nabla \boldsymbol{v} = -\frac{1}{\rho}\nabla P + \mathbf{g} + \nu \nabla^2 \boldsymbol{v}, \tag{2.13}$$

where $\nu = \mu/\rho$. These equations are called the Navier-Stokes equations. If viscous effects are negligible, which is generally found to be true far from boundaries of the flow field, (2.13) reduces to the Euler equation

$$\frac{\partial \boldsymbol{v}}{\partial t} + \boldsymbol{v} \cdot \nabla \boldsymbol{v} = -\frac{1}{\rho}\nabla P + \mathbf{g}. \tag{2.14}$$

## 2.2 Moving Mesh Methods

Over the last two decades many moving mesh methods have been developed to solve time-dependent PDEs with steep solutions. The aim of these methods is to find an efficient way for an automatic selection of meshes depending upon the behavior of the solution of the PDE. In the following two subsections we give a description of the

moving mesh methods based on the idea of the equidistribution principle, which was first introduced for differential equations by de Boor [14] and Dodson [15], and also give a summary of the GCL method described in [1].

Consider the initial-boundary value problem (IBVP)

$$u_t = f(u, u_x, u_{xx}) \tag{2.15a}$$

$$u(x,0) = g(x) \quad a \le x \le b, \quad u(a,t) = u_\alpha, \quad u(b,t) = u_\beta \quad t > 0. \tag{2.15b}$$

The following two approaches are often used to solve (2.15) numerically. The first approach is to use a finite difference scheme to discretize the PDE both in time and space on a fixed uniform spatial mesh. As a result of this discretization, we obtain an algebraic system of equations. The numerical solution of (2.15) will be obtained by solving the resulting algebraic system of equations. The second approach is by using the method of lines (MOL), in which the discretization is done in space or in time only. Discretizing in space produces a system of ordinary differential equations (ODEs) with appropriate boundary and initial conditions. The MOL approach separates the spatial and temporal variables which allows the possibility of using different meshes at different time levels. In the case of solving PDEs with steep solutions, a standard MOL approach in the variables $(x, t)$ requires the ODE solver to take very small time step to maintain accuracy. To resolve this problem, moving mesh methods are often used to obtain the numerical solution of the system (2.15). The idea behind moving mesh methods is to introduce new variables $(\xi, t)$ so that the given problem can be solved numerically easier than for the original variables $(x, t)$. The new variables are normally defined via a co-ordinate transformation, $x = x(\xi, t)$, $x \in [a, b]$, $t \ge 0$. The variables $(x, t)$ and $(\xi, t)$ are called the physical and computational variables respectively.

### 2.2.1 Equidistribution Method

The most commonly used moving mesh methods are based on the idea of equidistribution. Several moving mesh methods based on equidistribution principle have been developed in the literature (i.e., see [16], [18], [19], [13], [5], [8] and [1]).

The idea of equidistribution is as follows: Suppose some measure of the error function is available. Then, a good selection for a mesh

$$\pi : \{a = x_0(t) < x_1(t) < \cdots < x_{N-1}(t) < x_N(t) = b\}, \tag{2.16}$$

would be one where the contribution of the error function is distributed equally over the subintervals for all values of $t$. In practice, however, the mesh $\pi$ is found by approximately equidistributing with respect to the monitor function $M(x,t) > 0$. The arc-length monitor function

$$M(x,t) = \sqrt{1 + u_x^2}, \tag{2.17}$$

is commonly used to determine the distribution of the mesh at each time level. For example, the arc-length monitor function is used for the mesh selection to solve Burgers' equation (see [9])

$$u_t = [10^{-4}u_x - u^2/2]_x, \ -1 < x < 1, \ 0 < t \leq \pi/10, \tag{2.18a}$$

$$u(-1,t) = u(1,t) = 0, \quad u(x,0) = -\sin(\pi x). \tag{2.18b}$$

Figure 2.1 illustrates the mesh distribution and the solution of Burgers' equation (2.18) at time $t = \pi/10$. From figure 2.1 we notice that the mesh points are concentrated in the regions where the variation of the solution is large.

To obtain a mathematical expression for the EP we first assume, without loss of generality, that the computational co-ordinate lies in the unit interval [0,1], and a corresponding uniform mesh is given on the computational domain by

$$\xi_i = \frac{i}{N}, \quad i = 0, \ 1, \ 2, \ \ldots, \ N \tag{2.19}$$

Mathematically, finding moving meshes $\pi$ for which the monitor function $M$ is equally distributed for all values of $t$ means

$$\int_{x_{i-1}(t)}^{x_i(t)} M(x,t)\,dx = \frac{1}{N}\int_a^b M(x,t)\,dx =: \frac{1}{N}\theta(t), \quad i = 1, \ldots, N. \tag{2.20}$$

This equidistribution equation can be rewritten as

$$\int_a^{x_i(t)} M(x,t)\,dx = \frac{i}{N}\int_a^b M(x,t)\,dx = \frac{i}{N}\theta(t), \quad i = 0, \ldots, N. \tag{2.21}$$

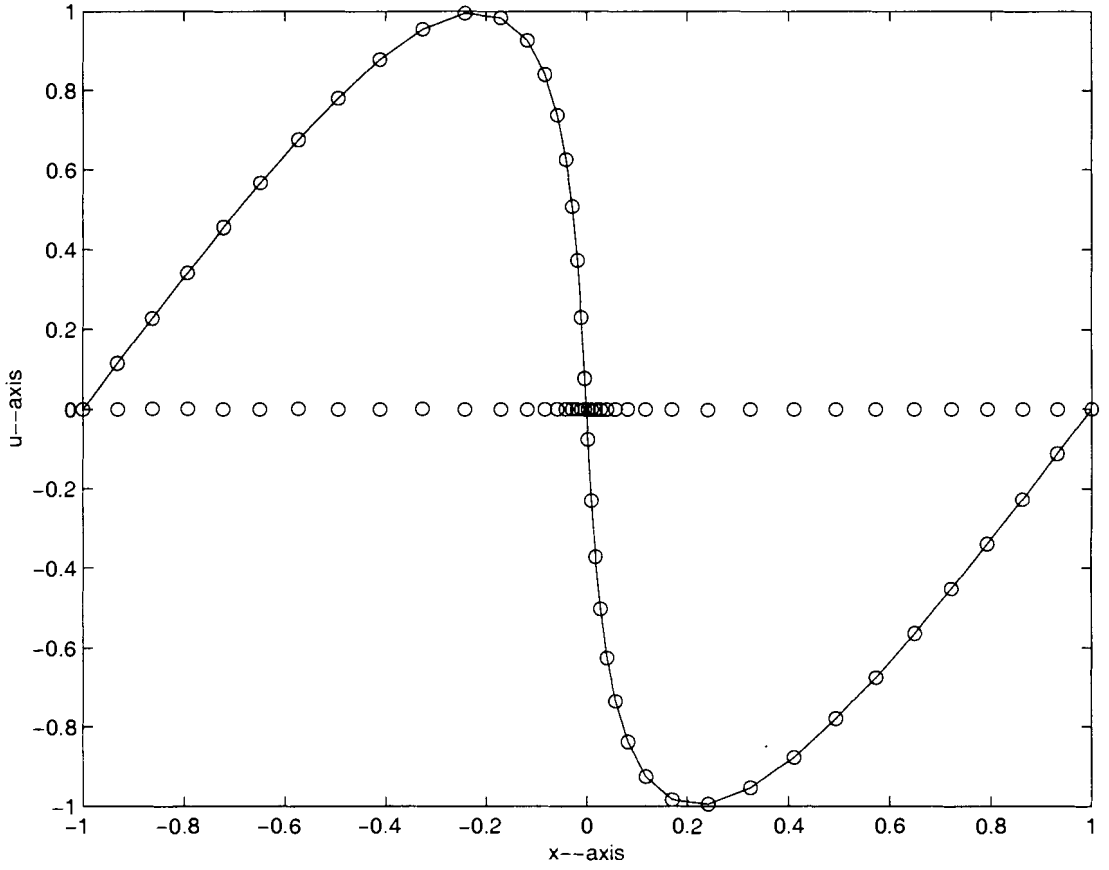


Figure 2.1: The solution of Burgers' equation and the distribution of the mesh points at $t = \pi/10$ using the arc-length monitor function.

From (2.19) and (2.21) follows the continuous form of EP

$$\xi\theta(t) = \int_a^x M(s,t)\,ds. \tag{2.22}$$

For notational simplicity, the explicit dependence of $M$ on $u$ is not specified. Differentiate (2.22) with respect to $\xi$ to obtain

$$M(x(\xi,t),t)\frac{\partial}{\partial\xi}x(\xi,t) = \theta(t), \tag{2.23}$$

or equivalently

$$\frac{\partial x}{\partial\xi} = \frac{\theta(t)}{M(x(\xi,t),t)}, \tag{2.24}$$

and then differentiate (2.23) with respect to $\xi$ to get

$$\frac{\partial}{\partial\xi}\Big\{M(x(\xi,t),t)\frac{\partial}{\partial\xi}x(\xi,t)\Big\} = 0. \tag{2.25}$$

The differential forms of the equidistribution principle (2.23) and (2.25) can be used to obtain the moving mesh $\{x_i(\xi,t)\}_{i=0}^N$. In [9] several other forms of moving mesh partial differential equations (MMPDEs) have been formulated from (2.22), (2.23) and (2.25) by differentiation with respect to time.

Differentiating the equidistribution equation (2.22) with respect to time along lines where $\xi(t)$ is constant yields

$$\xi_t\,\theta + \xi\,\dot\theta = \xi\,\dot\theta = \int_a^x \frac{\partial M}{\partial t}(s,t)\,ds + M\dot x. \tag{2.26}$$

Differentiate (2.26) with respect to $x$ to get

$$\xi_x\dot\theta + \xi\dot\theta_x = \xi_x\dot\theta = \frac{\partial M}{\partial t}(x,t) + \frac{\partial}{\partial x}(M\dot x). \tag{2.27}$$

Note that we have used Leibniz's rule in computing the right hand side of (2.26) and (2.27). Combining (2.24) and (2.27) gives

$$\frac{\partial}{\partial t}M(x,t) + \frac{\partial}{\partial x}(M(x,t)\dot x) = \frac{\dot\theta}{\theta}M(x,t), \tag{2.28}$$

or

$$\frac{\partial}{\partial t}M + \mathrm{div}(M\dot x) = \frac{\dot\theta}{\theta}M. \tag{2.29}$$

Define a normalized monitor function as

$$\frac{M(x,t)}{\int_a^b M(x,t)dx} = \frac{M(x,t)}{\theta} := \rho(x,t). \tag{2.30}$$

Rearranging (2.30) gives

$$M = \rho\theta. \tag{2.31}$$

Taking the time derivative of (2.31) yields

$$\frac{\partial M}{\partial t} = \frac{\partial \rho\theta}{\partial t} = \theta\frac{\partial \rho}{\partial t} + \dot{\theta}\,\rho. \tag{2.32}$$

Taking the derivative of $M\,\dot{x}$ with respect to $x$ gives

$$\frac{\partial}{\partial x}(M\dot{x}) = \frac{\partial}{\partial x}(\rho\theta\dot{x}) = \theta\frac{\partial}{\partial x}(\rho\dot{x}) = \theta\,\mathrm{div}(\rho\dot{x}). \tag{2.33}$$

Substituting (2.30), (2.32) and (2.33) into (2.29) yields

$$\frac{\partial}{\partial t}\rho + \mathrm{div}(\rho\dot{x}) = 0. \tag{2.34}$$

Note that (2.34) is just the conservation of mass equation found in fluid dynamics, where $\rho$ is interpreted as density. Thus, mesh points can be treated as particles in a flow. Furthermore, this suggests that it is meaningful to construct a moving mesh strategy based on conservation laws found in fluid dynamics.

### 2.2.2 The GCL Method

The MMPDEs (2.23) and (2.25) directly control the *location* of mesh points. Another class of moving mesh methods is the *velocity* based moving mesh methods. These methods control the time derivative of the mesh $\boldsymbol{x}(\boldsymbol{\xi}, t)$. Velocity based methods include the moving finite element method described in [10] and [11], the deformation method [12], and the GCL method [1]. For a velocity based method, the MMPDEs can be formulated for the mesh velocity. The mesh points are then obtained by integrating the mesh velocity field. In this subsection, we summarize the GCL method derived by Cao, Huang and Russell [1].

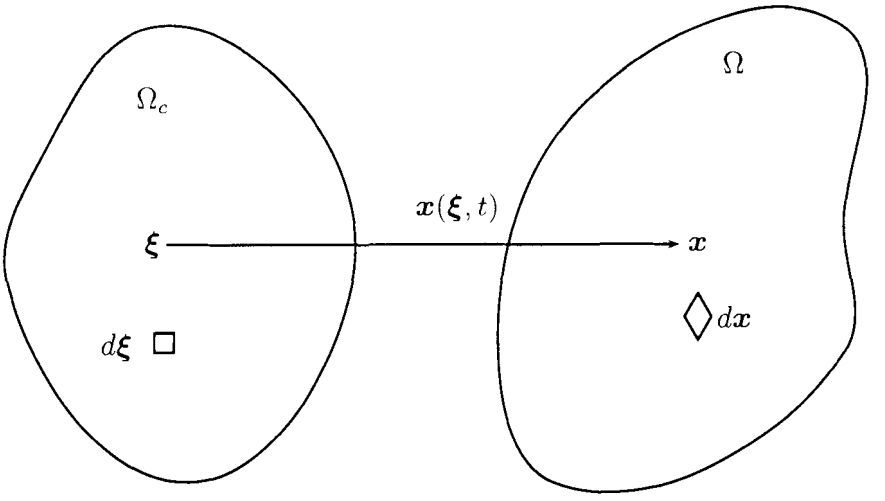


Figure 2.2: The mapping from $\Omega_c$ to $\Omega$

Consider a problem of solving a time-dependent PDE defined over a physical domain $\Omega \subset \mathbb{R}^n$, $n = 1$, 2 or 3. In order to obtain a numerical solution of the PDE using moving mesh methods, an automatic selection of an adaptive mesh at each time step is required. To this end, define a one-to-one co-ordinate transformation from a computational domain $\Omega_c \subset \mathbb{R}^n$ to the physical domain $\Omega$ (see figure 2.2)

$$\boldsymbol{x} : \Omega_c \rightarrow \Omega. \quad \boldsymbol{x}(\boldsymbol{\xi}, t) = \boldsymbol{x} \quad \forall \boldsymbol{\xi} \in \Omega_c. \tag{2.35}$$

Let $A_c$ be an arbitrary, fixed volume in $\Omega_c$ enclosed by a smooth boundary $\partial A_c$, and let $A(t) = \{\boldsymbol{x} | \boldsymbol{x} = \boldsymbol{x}(\boldsymbol{\xi}, t) \ \ \boldsymbol{\xi} \in A_c\}$ be the corresponding image of $A_c$ in $\Omega$ under the transformation $\boldsymbol{x} = \boldsymbol{x}(\boldsymbol{\xi}, t)$. Then the change in volume of $A(t)$ equals the total flux through the surface $\partial A(t)$

$$\frac{\mathrm{d}}{\mathrm{d}t} \int_{A(t)} d\boldsymbol{x} = \int_{\partial A(t)} \boldsymbol{x}_t \cdot \mathbf{n} \, dS, \tag{2.36}$$

where $\boldsymbol{x}_t$ is the mesh velocity. Equation (2.36) is the integral form of the geometric conservation law (GCL) derived by Thomas and Lombard [4] in the context of fluid dynamics. The left-hand side of (2.36) can be rewritten as

$$\frac{\mathrm{d}}{\mathrm{d}t} \int_{A(t)} d\boldsymbol{x} = \frac{\mathrm{d}}{\mathrm{d}t} \int_{A_c} \mathrm{J}(\boldsymbol{\xi}, t) \, d\boldsymbol{\xi} = \int_{A_c} \frac{D}{Dt} \mathrm{J}(\boldsymbol{\xi}, t) \, d\boldsymbol{\xi}, \tag{2.37}$$

where J is the Jacobian of the transformation, which gives the ratio of the volume element in $\Omega$ to volume element in $\Omega_c$, and $\frac{D}{Dt}$ is the time derivative in the co-ordinate system $(\boldsymbol{\xi}, t)$, and has the form

$$\frac{D}{Dt} = \frac{\partial}{\partial t} + \boldsymbol{x}_t \cdot \nabla, \tag{2.38}$$

where $\nabla$ is spatial gradient operator and $\partial/\partial t$ is the time derivative when $\boldsymbol{x}$ is fixed. Using the divergence theorem, the right-hand side of (2.36) can be written as

$$\int_{\partial A(t)} \boldsymbol{x}_t \cdot \mathbf{n}\, dS = \int_{A(t)} \nabla \cdot \boldsymbol{x}_t\, d\boldsymbol{x} = \int_{A_c} (\nabla \cdot \boldsymbol{x}_t)\mathrm{J}(\boldsymbol{\xi}, t)\, d\boldsymbol{\xi}. \tag{2.39}$$

Since $A_c$ is an arbitrary test volume, (2.36) gives the differential form of the GCL,

$$\nabla \cdot \boldsymbol{x}_t = \frac{1}{\mathrm{J}} \frac{D\mathrm{J}}{Dt}. \tag{2.40}$$

Suppose we are given a density function $\rho(\boldsymbol{x}, t) > 0$ such that

$$\int_{\Omega} \rho(\boldsymbol{x}, t)\, d\boldsymbol{x} = 1,$$

where $\rho(\boldsymbol{x}, t)$ is proportional to the variation in the solution of the underlying problem. Based on the one-dimensional equidistribution equation (2.24) discussed in Subsection § 2.2.1, for mesh adaptation it is reasonable to choose the Jacobian

$$\mathrm{J}(\boldsymbol{\xi}, t) = \frac{c(\boldsymbol{\xi})}{\rho(\boldsymbol{x}(\boldsymbol{\xi}), t)}, \tag{2.41}$$

where $c(\boldsymbol{\xi})$ is a time-independent function which can be determined from the initial co-ordinate transformation.

In particular, in one dimension (2.41) reduces to the equidistribution equation (2.24) when taking $c(\boldsymbol{\xi})$ =1. This means that (2.41) can be viewed as a generalization of the one-dimensional equidistribution principle.

Differentiate (2.41) with respect to time $t$ to get

$$\frac{\partial \mathrm{J}}{\partial t} = -\frac{c}{\rho^2} \frac{\partial \rho}{\partial t}, \tag{2.42}$$

and differentiating (2.41) with respect to $\boldsymbol{x}$ gives

$$\nabla \mathrm{J} = -\frac{c}{\rho^2} \nabla \rho. \tag{2.43}$$

Using (2.38) we obtain

$$\frac{D\mathrm{J}}{Dt} = \frac{\partial \mathrm{J}}{\partial t} + \boldsymbol{x}_t \cdot \nabla \mathrm{J}. \tag{2.44}$$

Substituting (2.42) and (2.43) into (2.44) gives

$$\frac{D\mathrm{J}}{Dt} = -\frac{c}{\rho^2}\left(\frac{\partial \rho}{\partial t} + \boldsymbol{x}_t \cdot \nabla \rho\right), \tag{2.45}$$

which is equivalent to

$$\frac{D\mathrm{J}}{Dt} = -\frac{c}{\rho^2}\frac{D\rho}{Dt}, \tag{2.46}$$

so that

$$\frac{1}{\mathrm{J}}\frac{D\mathrm{J}}{Dt} = \left(\frac{\rho}{c}\right)\left(\frac{-c}{\rho^2}\frac{D\rho}{Dt}\right) = -\frac{1}{\rho}\frac{D\rho}{Dt}. \tag{2.47}$$

Using (2.47) we can rewrite the differential form of the GCL (2.40) as

$$\nabla \cdot \boldsymbol{x}_t = -\frac{1}{\rho}\frac{D\rho}{Dt} = -\frac{1}{\rho}\left(\frac{\partial \rho}{\partial t} + \boldsymbol{x}_t \cdot \nabla \rho\right), \tag{2.48}$$

or equivalently,

$$\frac{\partial \rho}{\partial t} + \nabla \cdot (\rho \boldsymbol{x}_t) = 0. \tag{2.49}$$

Note that (2.49) is mathematically equivalent to (2.41) since (2.41) is satisfied by any nonsingular transformation, and (2.49) is just the conservation of mass equation in fluid dynamics. Therefore, as seen in the one-dimensional space, for two- and three-dimensional spaces it is also meaningful to construct a moving mesh method based upon the conservation laws found in the literature of fluid dynamics.

Suppose the physical domain $\Omega$ does not move with time. Integrating (2.49) over $\Omega$ and using the divergence theorem we obtain

$$\int_\Omega \frac{\partial \rho}{\partial t}\, d\boldsymbol{x} + \int_\Omega \nabla \cdot (\rho \boldsymbol{x}_t)\, d\boldsymbol{x} = \frac{\mathrm{d}}{\mathrm{d}t}\int_\Omega \rho\, d\boldsymbol{x} + \int_{\partial\Omega} \rho \boldsymbol{x}_t \cdot \mathbf{n}\, dS = 0, \tag{2.50}$$

where $\mathbf{n}$ is a unit vector normal to $\partial\Omega$. If we assume that the boundary points are not allowed to move out of the physical domain,

$$\boldsymbol{x}_t \cdot \mathbf{n} = 0 \quad \text{on } \partial\Omega, \tag{2.51}$$

so the boundary term in (2.50) vanishes. Thus, (2.50) gives the compatibility condition

$$\frac{\mathrm{d}}{\mathrm{d}t}\int_\Omega \rho(\boldsymbol{x}, t)\, d\boldsymbol{x} = 0. \tag{2.52}$$

Using the Helmholtz's decomposition theorem 1.2, Cao, Huang and Russell [1] show that the mesh velocity field can be determined using the additional condition

$$\nabla \times w(\boldsymbol{v} - \boldsymbol{u}) = 0 \quad \text{in } \Omega, \tag{2.53}$$

where $w$ and $\boldsymbol{u}$ are, respectively, a weight function and a background velocity field to be specified, and $\boldsymbol{v}$ is the mesh velocity field which was previously denoted by $\boldsymbol{x}_t$. Equivalently, (2.53) can be rewritten as

$$\boldsymbol{v} = \boldsymbol{u} + \frac{1}{w}\nabla\phi, \tag{2.54}$$

where $\phi$ is a smooth potential function. In terms of the notation $\boldsymbol{v}$ for the mesh velocity, the boundary condition (2.51) can be rewritten as

$$\boldsymbol{v} \cdot \mathbf{n} = 0 \quad \text{on } \partial\Omega. \tag{2.55}$$

Substituting (2.54) into (2.49) and (2.55) yields the elliptic system

$$\nabla \cdot \left(\frac{\rho}{w}\nabla\phi\right) = -\frac{\partial\rho}{\partial t} - \nabla \cdot (\rho\boldsymbol{u}) \quad \text{in } \Omega, \tag{2.56a}$$

$$\frac{\partial\phi}{\partial n} = -w\boldsymbol{u} \cdot \mathbf{n} \quad \text{on } \partial\Omega. \tag{2.56b}$$

Solving the system (2.56) for $\phi$, the mesh $\boldsymbol{x} = \boldsymbol{x}(\boldsymbol{\xi}, t)$ can then be determined from the initial mesh $\boldsymbol{x}(\boldsymbol{\xi}, 0)$ by time integration of the velocity field

$$\boldsymbol{x}_t = \boldsymbol{u}(\boldsymbol{x}, t) + \frac{1}{w(\boldsymbol{x}, t)}\nabla\phi(\boldsymbol{x}, t). \tag{2.57}$$

In [1] (2.49) and (2.53) are shown to be exactly the Euler Lagrange equations for the least square functional

$$I(\boldsymbol{v}) = \frac{1}{2}\int_\Omega \left\{ \left| \nabla \cdot (\rho\boldsymbol{v}) + \frac{\partial\rho}{\partial t} \right|^2 + \left(\frac{\rho}{w}\right)^2 |\nabla \times w(\boldsymbol{v} - \boldsymbol{u})|^2 \right\} d\boldsymbol{x}, \tag{2.58}$$

where the minimization is over all vector fields $\boldsymbol{v}(\boldsymbol{x}, t)$ that satisfy the boundary condition (2.55). Thus, the velocity field can be computed directly by minimizing the functional $I(\boldsymbol{v})$ in (2.58), and the mesh can be found by solving

$$\boldsymbol{x}_t(\boldsymbol{\xi}, t) = \boldsymbol{v}(\boldsymbol{x}(\boldsymbol{\xi}, t), t), \quad \boldsymbol{\xi} \in \Omega_c \tag{2.59}$$

## 2.3 Mass Transfer Problem

The mass transfer problem was first described by Monge in 1781. It was formulated as a problem of displacing parcel material from one site to another one with minimal transportation cost. This problem was later studied by Kantorovich in 1942 (see [6]), leading to the so-called Monge-Kantorovich problem (MKP) which has applications in many different fields. Benamou and Brenier [2] formulate MKP in a computational fluid mechanics framework. In this Section, we give a summary of the MKP framework described in [2]. The Monge-Kantorovich mass transfer problem is stated as follows:

Given two density functions $\rho_0(\boldsymbol{x}) > 0$, $\rho_T(\boldsymbol{x}) > 0 \forall\, \boldsymbol{x} \in \mathbb{R}^n$, with total mass one, i.e.,

$$\int_{\mathbb{R}^n} \rho_0(\boldsymbol{\xi})\, d\boldsymbol{\xi} = \int_{\mathbb{R}^n} \rho_T(\boldsymbol{x})\, d\boldsymbol{x} = 1, \tag{2.60}$$

determine a mapping $\boldsymbol{x} : \mathbb{R}^n \rightarrow \mathbb{R}^n, \boldsymbol{x} = \boldsymbol{x}(\boldsymbol{\xi}, t)$ such that

$$\int_{\boldsymbol{x}^{-1}(\Omega)} \rho_0(\boldsymbol{\xi})\, d\boldsymbol{\xi} = \int_{\Omega} \rho_T(\boldsymbol{x})\, d\boldsymbol{x} \tag{2.61}$$

for all bounded subsets $\Omega$ of $\mathbb{R}^n$.

If $\boldsymbol{x}(\boldsymbol{\xi}, t)$ is a smooth and one to one mapping, then (2.61) gives

$$\int_{\Omega} \rho_T(\boldsymbol{x})\, d\boldsymbol{x} = \int_{\boldsymbol{x}^{-1}(\Omega)} \rho_T\left(\boldsymbol{x}\left(\boldsymbol{\xi}\right)\right) \det\left(\frac{\partial \boldsymbol{x}\left(\boldsymbol{\xi}\right)}{\partial \boldsymbol{\xi}}\right) d\boldsymbol{\xi}. \tag{2.62}$$

Since $\Omega$ is arbitrarily chosen, (2.61) and (2.62) give

$$\mathrm{J} = \det\left(\frac{\partial \boldsymbol{x}\left(\boldsymbol{\xi}\right)}{\partial \boldsymbol{\xi}}\right) = \frac{\rho_0(\boldsymbol{\xi})}{\rho_T\left(\boldsymbol{x}\left(\boldsymbol{\xi}\right)\right)}, \tag{2.63}$$

where J is the determinant of the Jacobian matrix which describes the rate of compression or spreading of the mass induced by the mapping $\boldsymbol{x} : \boldsymbol{\xi} \rightarrow \boldsymbol{x}(\boldsymbol{\xi})$.

The selection of the mapping $\boldsymbol{x}(\boldsymbol{\xi})$ that satisfies (2.63) is not unique. To show this non-uniqueness, for instance, if we take $\Omega_c = \Omega = B_1(0,0)$ (the unit circle with center $(0,0)$), then

$$\boldsymbol{x}_k(r,\theta) = \left(r\, \cos\left(\theta + 2k\pi r^2\right), r\, \sin\left(\theta + 2k\pi r^2\right)\right)\ \ k = 1,\, 2,\, 3 \ldots$$

satisfy (2.63) with $\rho_0/\rho_T = 1$. Therefore, the mapping which satisfies (2.63) can be selected to be optimal in a suitable sense. One way is to introduce the $L^p$ Kantorovich (or Wasserstein) distance between $\rho_0$ and $\rho_T$ defined as

$$d_p(\rho_0, \rho_T)^p = \inf_{\boldsymbol{x}} \int |\boldsymbol{x}(\boldsymbol{\xi}) - \boldsymbol{\xi}|^p \rho_0(\boldsymbol{\xi}) d\boldsymbol{\xi}, \tag{2.64}$$

where $p \geq 1$ is fixed, $|\cdot|$ denotes the Euclidean norm in $\mathbb{R}^n$ and the infimum is taken among all maps $\boldsymbol{x}(\boldsymbol{\xi})$ transporting $\rho_0$ to $\rho_T$. The original Monge transfer problem corresponds to $p = 1$. The case $p = 2$ has been studied by Benamou and Brenier [2].

**Definition 2.1.** The mapping $\boldsymbol{x} = \boldsymbol{x}(\boldsymbol{\xi})$ is said to be an optimal mapping and solves the $L^p$ Monge-Kantorovich problem (MKP) if the infimum in (2.64) is achieved by the map $\boldsymbol{x} = \boldsymbol{x}(\boldsymbol{\xi})$.

□

This definition concludes that the Monge-Kantorovich problem consists of finding a mapping $\boldsymbol{x} = \boldsymbol{x}(\boldsymbol{\xi})$ which satisfies (2.63) and minimizes the transportation cost

$$C(\boldsymbol{x}) = \int_{\mathbb{R}^n} |\boldsymbol{x}(\boldsymbol{\xi}) - \boldsymbol{\xi}|^2 \rho_0(\boldsymbol{\xi}) d\boldsymbol{\xi} \tag{2.65}$$

where $|\boldsymbol{x}(\boldsymbol{\xi}) - \boldsymbol{\xi}|^2 \rho_0(\boldsymbol{\xi})$ is the traveled squared distance weighted by the amount of the transferred mass. In the following, we state the basic theoretical result of the $L^2$MKP (see [7], [3]).

**Theorem 2.1.** There is a unique optimal transfer $\hat{\boldsymbol{x}} = \hat{\boldsymbol{x}}(\boldsymbol{\xi}, t)$ characterized as the unique mapping which transfers $\rho_0$ to $\rho_T$ and can be written as a gradient of a convex function $\Psi$

$$\hat{\boldsymbol{x}}(\boldsymbol{\xi}, t) = \nabla \Psi(\boldsymbol{\xi}). \tag{2.66}$$

□

Substituting (2.66) into (2.63) shows that $\Psi$ is a solution (in a suitable weak sense) of the Monge-Ampere equation

$$\det\left(H\Psi(\boldsymbol{\xi})\right) \rho_T\left(\nabla \Psi(\boldsymbol{\xi})\right) = \rho_0(\boldsymbol{\xi}), \tag{2.67}$$

where $H\Psi$ is the Hessian matrix of $\Psi$. Therefore, the solution of the Monge-Kantorovich mass transfer problem reduces to solving the Monge-Ampere equation (2.67).

To avoid solving equation (2.67) directly, Benamou and Brenier [2] introduce an alternative numerical method for the $L^2$MKP based on transforming the mass transfer problem into a continuum mechanics framework. To establish this framework they artificially fix a time interval [0,T] and consider all possible smooth enough, time-dependent, density and velocity fields $\rho(\boldsymbol{x},t) > 0, \boldsymbol{v}(\boldsymbol{x},t) \in \mathbb{R}^n$ that satisfy the continuity equation

$$\frac{\partial \rho}{\partial t} + \nabla \cdot (\rho \boldsymbol{v}) = 0, \tag{2.68}$$

for $0 \leq t \leq T$, $\boldsymbol{x} \in \mathbb{R}^n$ , with initial and final conditions

$$\rho(\cdot,0) = \rho_0, \quad \rho(\cdot,T) = \rho_T. \tag{2.69}$$

The new problem then is to minimize the functional

$$C(\rho,\boldsymbol{v}) = T \int_0^T \int_{\mathbb{R}^n} \rho(\boldsymbol{x},t)\,|\boldsymbol{v}(\boldsymbol{x},t)|^2\,d\boldsymbol{x}\,dt, \tag{2.70}$$

for all $(\rho,\boldsymbol{v})$ satisfying (2.68) and (2.69).

The relationship between the Monge-Kantorovich problem and continuum fluid mechanics is established through the following proposition [2].

**Proposition 2.1.** The square of the $L^2$ Kantorovich distance is equal to the infimum of the functional

$$T \int_0^T \int_{\mathbb{R}^n} \rho(\boldsymbol{x},t)\,|\boldsymbol{v}(\boldsymbol{x},t)|^2\,d\boldsymbol{x}dt, \tag{2.71}$$

among all $(\rho,\boldsymbol{v})$ satisfying (2.68) and (2.69).

There exists moreover a unique optimal flow written as

$$\partial_t \boldsymbol{x} = \boldsymbol{v}(\boldsymbol{x}(\boldsymbol{\xi},t),t), \quad \boldsymbol{x}(\boldsymbol{\xi},0) = \boldsymbol{\xi}\ \forall \boldsymbol{\xi}.$$

In terms of the potential $\Psi$ the flow is given as

$$\boldsymbol{x}(\boldsymbol{\xi},t) = \boldsymbol{x} + \frac{t}{T}(\nabla\Psi - \boldsymbol{x}).$$

□

The optimality conditions of this space-time minimization problem are shown to be (see [2])

$$\boldsymbol{v}(\boldsymbol{x},t) = \nabla\phi(\boldsymbol{x},t), \tag{2.74}$$

and the Hamilton-Jacobi equation

$$\partial_t\phi + \frac{1}{2}|\nabla\phi|^2 = 0, \tag{2.75}$$

where the potential $\phi$ is the Lagrange multiplier of the constraints (2.68) and (2.69).

## 2.4 Semi-geostrophic Equations

The semi-geostrophic equations are the standard model for slowly varying flows constrained by rotation and stratification. They have been used to describe front formation in meteorology. In this section we give a summary of the semi-geostrophic equations studied by Purser and Cullen [38].

For a constant Coriolis force $f$, the semi-geostrophic equations can be written as (see [34], [38], [36])

$$\frac{Du_g}{Dt} - fv + \frac{\partial\psi}{\partial x} = \frac{Du_g}{Dt} - f(v - v_g) = 0, \tag{2.76a}$$

$$\frac{Dv_g}{Dt} + fu + \frac{\partial\psi}{\partial y} = \frac{Dv_g}{Dt} + f(u - u_g) = 0, \tag{2.76b}$$

$$\frac{D\theta}{Dt} = 0, \tag{2.76c}$$

$$\nabla_x \cdot \boldsymbol{u} = 0, \tag{2.76d}$$

$$\nabla_x\psi = \left(\frac{\partial}{\partial x}, \frac{\partial}{\partial y}, \frac{\partial}{\partial z}\right)\psi = \left(fv_g, -fu_g, g\frac{\theta}{\theta_0}\right), \tag{2.76e}$$

where $(u_g, v_g)$ is the geostrophic wind, $\theta$ is the potential temperature, $\psi$ is the geopotential and $g$ is the acceleration due to gravity.

The system (2.76) can be solved by defining the co-ordinate transformation (see [36])

$$\boldsymbol{X} \equiv (X, Y, Z)^T = \left(x + \frac{v_g}{f}, y - \frac{u_g}{f}, \frac{g\theta}{f^2\theta_0}\right)^T. \tag{2.77}$$

The transformation (2.77) describes the evolution of a spatial mesh. Using (2.77), the semi-geostrophic equations (2.76a) , (2.76b) and (2.76c) reduces to the Lagrangian form

$$\frac{D\boldsymbol{X}}{Dt} = \boldsymbol{u}_g \equiv (u_g, v_g, 0)^T. \tag{2.78}$$

It is shown that the Jacobian of the transformation (2.77) defined as

$$q = \det\left(\frac{\partial(X, Y, Z)}{\partial(x, y, z)}\right), \tag{2.79}$$

satisfies

$$\frac{D\,q}{D\,t} = 0. \tag{2.80}$$

Using (2.76e), the transformation (2.77) can be written as

$$\boldsymbol{X} = \nabla_x P, \tag{2.81}$$

where

$$P(\boldsymbol{x}) = \frac{\psi}{f^2} + \frac{1}{2}(x^2 + y^2). \tag{2.82}$$

The transformation (2.77) is due to Hoskins [36]. Substituting (2.81) into (2.79) gives the Monge-Ampere equation

$$q = \det(H_x P), \tag{2.83}$$

where $H_x P$ is the Hessian of $P$ with respect to coordinates $\boldsymbol{x}$. The Hessian of $P$ is symmetric, and if it is nonsingular its inverse is also symmetric. This implies that $\boldsymbol{x}$ is the gradient of some function $R(\boldsymbol{X})$, i.e.,

$$\boldsymbol{x} = \nabla_X R \tag{2.84}$$

where

$$\nabla_X = \left(\frac{\partial}{\partial X}, \frac{\partial}{\partial Y}, \frac{\partial}{\partial Z}\right).$$

$R$ is called the Legendre conjugate convex function of $P$, and they can be shown to be related by (see [37])

$$P + R = \boldsymbol{x} \cdot \boldsymbol{X}. \tag{2.85}$$

From (2.77) and (2.84) we get

$$u_g = f\left(\frac{\partial R}{\partial Y} - Y\right), \quad v_g = -f\left(\frac{\partial R}{\partial X} - X\right). \tag{2.86}$$

Taking $\rho = 1/q$, i.e., $\rho$ has a meaning of density, then from (2.79) and (2.84) we obtain the Monge-Ampere equation

$$\rho = det(H_X\, R). \tag{2.87}$$

It can be shown that

$$\frac{D_X \rho}{Dt} = 0, \tag{2.88}$$

where

$$\frac{D_X}{Dt} = \frac{\partial}{\partial t} + \boldsymbol{u}_g \cdot \nabla_X. \tag{2.89}$$

The velocity field $(u_g, v_g)$ then can be computed as follows:

1. Given the values of $\rho$ at $t = 0$, solve the Monge-Ampere equation (2.87) for $R$
2. Calculate the velocity field $(u_g, v_g)$ from $R$ using (2.86)
3. From (2.88) compute a new density $\rho$ using the values of the just calculated velocity $(u_g, v_g)$, and return to 1.

## 2.5 Computational Anatomy

Miller et al. [24] show that there are three aspects of Computational Anatomy (CA):

1. Automated construction of anatomical manifolds, points, curves, surfaces and subvolumes.
2. Comparison of these manifolds.
3. Statistical codification of variability of anatomy via probability measures allowing for inference and hypothesis testing of disease states.

**Definition 2.2.** Mathematical structures are termed as anatomies in CA.

□

In [24] it is shown that the study of the second aspect of CA is based on the theory of transformations. There are two types of transformations that have been studied in the literature of CA:

1. Geometric or shape type studied through mappings of the co-ordinate systems of the anatomies. Variation in the image space is accommodated by introducing groups of transformations carrying individual elements from one site to another.

2. The second transformations type is of photometric values accommodating the appearance or creation of new structures.

Dupuis et al. [27] and Trouve [26] (see also [24], [25]) established a variational formulation of the basic transformation problem. We review their findings in this Section.

The mappings of shape type are invertible, 1-1, onto continuous mappings with continuous inverses that are differentiable (i.e., diffeomorphisms). These transformations form a group denoted by $\mathcal{X}$.

Let the background space $\Omega$ be a bounded domain with a piecewise $C^1$ boundary on $\mathbb{R}^n$. Define the transformations $\boldsymbol{x}(t) \in \mathcal{X} : \Omega \rightarrow \Omega, \quad t \in [0,1]$.

The inverse transformations $\boldsymbol{x}^{-1}(t) = \boldsymbol{\xi}(t)$ are uniquely defined according to

$$\boldsymbol{x}^{-1}(\boldsymbol{x}(\boldsymbol{\xi},t),t) = \boldsymbol{\xi}(\boldsymbol{x}(\boldsymbol{\xi},t),t) = \boldsymbol{\xi}, \quad t \in [0,1]. \tag{2.90}$$

The evolution equations of $\boldsymbol{x}(t)$ and its inverse $\boldsymbol{\xi}(t)$ can be written as (see [24])

$$\frac{\partial}{\partial t}\boldsymbol{x}(\boldsymbol{\xi},t) = \boldsymbol{v}(\boldsymbol{x}(\boldsymbol{\xi},t),t), \tag{2.91a}$$

$$\frac{\partial}{\partial t}\boldsymbol{\xi}(\boldsymbol{x},t) = -D\boldsymbol{\xi}(\mathbf{x},\mathbf{t})\boldsymbol{v}(\boldsymbol{x},t), \tag{2.91b}$$

$$\boldsymbol{x}(0) = \boldsymbol{\xi}(0) = id, \tag{2.91c}$$

where $id$ is the identity map and $D$ is the Jacobian matrix of the inverse transformation $\boldsymbol{\xi}(\boldsymbol{x},t)$, giving an $n \times n$ matrix for $\mathbb{R}^n$ valued function $f$,

$$Df_{ij} = \frac{\partial f_i}{\partial x_j}.$$

Figure 2.3 shows the description of the evolution equations (2.91) and the variation of the flows $\boldsymbol{x}(\cdot)$.

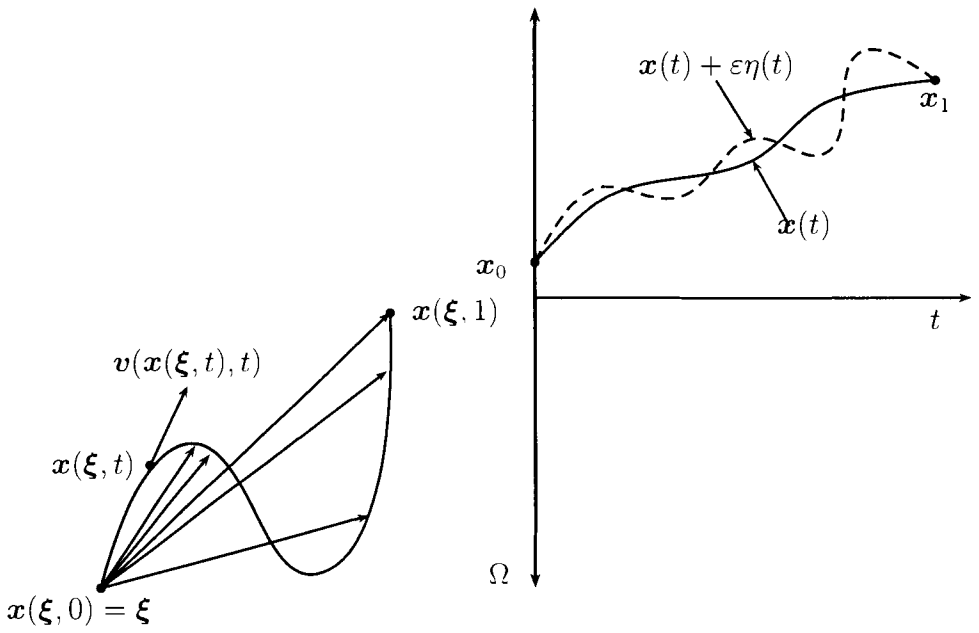


Figure 2.3: The figure on the left shows the Lagrangian description of the flow; The figure on the right shows the variation of the flow element $\boldsymbol{x}(\cdot)$ by $\eta(\cdot)$.

**Remark 2.1.** Note that in the moving mesh context the notation J has been used for the determinant of the Jacobian matrix, i.e., in CA

$$\mathrm{J} = \det D.$$

□

An essential aspect of CA is to define the metric distance between anatomies through the mapping between them. In [27], [24] and [26] the distance between two anatomies is defined via the geodesic length of the flows that connect them.

**Definition 2.3.** The geodesic length is defined as the square root of the energy of the transformation of the path

$$E(\boldsymbol{x}) = \int_0^1 \|\boldsymbol{v}(t)\|_L^2 dt, \quad \boldsymbol{v}(t) = \frac{\partial \boldsymbol{x}}{\partial t}, \tag{2.93}$$

where $\|\cdot\|_L$ is a suitable norm defined on $\Omega$ (e.g., a Sobolev space with $L$ a differential operator). In practice, linear differential operators have been used to enforce smoothness on maps; it is generally constructed from the Laplacian and its powers. In $\mathbb{R}^n$, $L$ is an $n \times n$ matrix of differential operators $L = (L_{ij})$ defined as

$$L\boldsymbol{v}(\cdot, t) = \sum_{i=1}^{n} L_{ij} v_i, j = 1, 2, \ldots, n.$$

The norm-square energy density is defined as

$$\begin{aligned} E_v(t) &= \int_\Omega E_v(\xi, t) d\xi = \|\mathbf{v}(\mathbf{t})\|_L^2 \\ &= (L\boldsymbol{v}(\cdot, t), L\boldsymbol{v}(\cdot, t)) < \infty, t \in [0, 1]. \end{aligned} \tag{2.94}$$

□

**Theorem 2.2.** The metric between transformations $\boldsymbol{x}(0), \boldsymbol{x}(1)$ is defined as the length of the shortest path $\boldsymbol{x}(t)$, $t \in [0, 1]$ satisfying (2.91b) with the boundary conditions $\boldsymbol{x}(0) = \boldsymbol{x}_0, \boldsymbol{x}(1) = \boldsymbol{x}_1$, i.e.,

$$d(\boldsymbol{x}_0, \boldsymbol{x}_1)^2 = \inf_{\boldsymbol{x}} \int_0^1 E_v(t) dt = \inf_{\boldsymbol{x}} \int_0^1 \|\boldsymbol{v}(t)\|_L^2 dt, \tag{2.95}$$

The geodesics satisfy the Euler-Lagrange equation (see [24])

$$\begin{aligned}\frac{\partial}{\partial t}\nabla_v E_v(\cdot,t) &+ (D\,\boldsymbol{v}(\cdot,t))^T\nabla_v E_v(\cdot,t) + (D\,\nabla_v E_v(\cdot,t))\boldsymbol{v}(.,t)\\ &+ \operatorname{div}\boldsymbol{v}(\cdot,t)\,\nabla_v E_v(\cdot,t) = 0,\end{aligned} \tag{2.96}$$

where $\nabla_v E_v(.,t) = 2L^*L\boldsymbol{v}(t)$ with the adjoint defined as $(L\boldsymbol{x}(1),\boldsymbol{x}(2)) = (\boldsymbol{x}(1),L^*\boldsymbol{x}(2))$, and div is the divergence operator.

□

**Remark 2.2.** Note that in one dimension equation (2.96) reduces to the Burgers' equation. In fact for $L = id, \nabla_v E_v = 2v$ and $Dv = (Dv)^T = \operatorname{div} v = v_x$, hence, (2.96) reduces to

$$\boldsymbol{v}_t + 3\boldsymbol{v}_x\boldsymbol{v} = 0. \tag{2.97}$$

□

Equation (2.96) was first derived by Mumford [35]. He used a variational argument to compute (2.96) via perturbing the geodesic by $\eta(t)$, $t \in [0,1]$ and leaving the endpoints unchanged (see Figure 2.3).

**Remark 2.3.** Note that the distance (2.95) has similar form as the $L^2$MKP distance (2.71) defined in Section 2.3.

□

**Definition 2.4.** Image functions in CA are defined as functions from the background space $\Omega$ to $\mathbb{R}^n$. $\mathrm{I}: \Omega \to \mathbb{R}^n$. For example, in MRI 8-bit gray-scale images,

$$\mathrm{I}(\boldsymbol{x}) \in [0,255], \quad \boldsymbol{x} \in \Omega = (0,1)^2\ (2D),\ (0,1)^3\ (3D).$$

□

Denote the set of all anatomical image functions by $\mathcal{I}$,

$$\mathcal{I} = \{\mathrm{I}' : \mathrm{I}'(\cdot) = \mathrm{I}(\boldsymbol{x}(\cdot)), \mathrm{I} \in \mathcal{I}\, \boldsymbol{x} \in \mathcal{X}\}.$$

For any two images $I_0, I_1 \in \mathcal{I}$, there exists a transformation $\boldsymbol{x}$ that registers the given images $I_1 = I_0(\boldsymbol{x})$. Given two anatomical images $I_0$ and $I_1$, identify the first image with the identity transformation and the second image, call it target image, with a transformation (to be estimated) $\boldsymbol{x}_1$. The deformable template model approach to image comparison involves estimation of the unknown diffeomorphism $\boldsymbol{x}_1$ registering the given images i.e., $I_1 = I_0 \circ \boldsymbol{x}_1$.

The goal in CA is essentially to construct the shortest length curve $\boldsymbol{x}(t), t \in [0,1]$ which connects two elements $I_0, I_1 \in \mathcal{I}$ and minimizes the target norm squared

$$\|I_0(\boldsymbol{\xi}(1)) - I_1\|^2.$$

This is called inexact matching which has been studied by Dupuis [27].

In the literature of medical imaging the *registration problem* is defined as the problem of determining the corresponding points between two images or between an image and the anatomy. In other words, *the registration problem* is a problem of constructing a coordinate transformations between the data sets. In [28] and [31] a method of registration based on the Monge-Kantorovich problem of optimal mass transport is derived.

# Chapter 3

# Links with Mesh Adaptivity Techniques

When using moving mesh methods to solve a time dependent PDE, it is generally required to find an automatic way of selecting an adaptive mesh which suits the behavior of the physical solution. The adaptive mesh is determined by constructing a time dependent co-ordinate transformation between a computational domain $\Omega_c$ and a physical domain $\Omega$. This co-ordinate transformation is determined by solving a set of moving mesh PDEs. In this Chapter, we present a relationship between the co-ordinate transformation techniques that have been used in moving mesh methods for the purpose of generating adaptive mesh and the co-ordinate transformation used in the Monge-Kantorovich mass transfer problem for the purpose of obtaining an optimal transport mapping. We also present some links between the transformational techniques of moving mesh methods and those found in some applications that are related to the Monge-Kantorovich problem; for example, fluid dynamics, meteorology, computational anatomy, and image registration.

## 3.1 Links with the Monge-Kantorovich Problem

The main purpose of this section is to establish a link between the transformations that have been used for solving the Monge-Katorovich mass transfer problem [2] and

the techniques of adaptivity for moving mesh methods.

Consider the mapping $\boldsymbol{x}(\boldsymbol{\xi}) = \boldsymbol{x}$ defined in the MKP formulation that transfers a density $\rho_0(\boldsymbol{\xi}) > 0$ defined on $\Omega_c$ to a density $\rho_T(\boldsymbol{x}) > 0$ defined on $\Omega$. To establish a link between this mapping and those transformational techniques of moving mesh methods, $\Omega_c$ and $\Omega$ can be thought of as a physical and computational domains, respectively, with $\rho_0$ being independent of time. Recall that from the MKP formulation (see section § 2.3) we have the condition

$$\int_{\Omega_c} \rho_0(\boldsymbol{\xi})\, d\boldsymbol{\xi} = \int_{\Omega} \rho_T(\boldsymbol{x})\, d\boldsymbol{x}. \tag{3.1}$$

Condition (3.1) states that the two domains $\Omega_c$ and $\Omega$ have the same amount of mass. Thus, this condition is equivalent to the compatibility condition (2.52) for the transformation defined in the GCL method to generate adaptive mesh.

For the mapping defined for the MKP, it is shown that its Jacobian has the form (see section § 2.3)

$$\mathrm{J} = \frac{\rho_0(\boldsymbol{\xi})}{\rho_T(\boldsymbol{x}(\boldsymbol{\xi}))}, \tag{3.2}$$

and (3.2) is shown to be equivalent to the Monge-Ampere equation

$$\det(H\Psi(\boldsymbol{\xi})) = \frac{\rho_0(\boldsymbol{\xi})}{\rho_T(\boldsymbol{x}(\boldsymbol{\xi}))}. \tag{3.3}$$

We first consider the one-dimensional problem. If we take $\rho_0 = 1$ and $\rho_T = M$, where $M$ is a monitor function, then equation (3.2) is just the equidistribution principle (2.24)

$$\mathrm{J} = \frac{1}{M}. \tag{3.4}$$

Moreover, using (3.2), (3.3) and (3.4), the optimal transport problem reduces to solving

$$\Psi_{\xi\xi} = \frac{1}{M}. \tag{3.5}$$

Finding a suitable monitor function $M$ is very problem dependent; for example, when solving the problem (2.15) with $f(x, u_x, u_{xx}) = \epsilon u_{xx} - u u_x$, the selected monitor function is the arc-length monitor function $M = \sqrt{1 + u_x^2}$. The optimal mapping

$x(\xi)$ can be obtained by solving (3.5) for $\Psi$ and then setting

$$x(\xi) = \frac{\partial}{\partial \xi}\Psi(\xi). \tag{3.6}$$

In two- or three-dimensions, a link between the mapping of the optimal transportation mapping and the technique of adaptivity can be established via the generalized form of the equidistribution principle (2.41) derived by Cao, Huang and Russell [1] (see Subsection § 2.2.2). This link can be shown by taking $\rho_0(\boldsymbol{\xi}) = c(\boldsymbol{\xi})$ and $\rho_T(\boldsymbol{x}) = \rho(\boldsymbol{x}, T)$, (3.2) reduces to the generalized form of the equidistribution principle (2.41)

$$\mathrm{J} = \frac{c}{\rho}. \tag{3.7}$$

Thus, the optimal transport mapping can be obtained by solving the Monge-Ampere equation

$$\det\left(H\Psi(\boldsymbol{\xi})\right) = \frac{c(\boldsymbol{\xi})}{\rho\left(\boldsymbol{x}\left(\boldsymbol{\xi}, T\right)\right)}. \tag{3.8}$$

The mesh velocity field in the GCL method formulation [1] is computed by using the Helmholtz's decomposition theorem [44] (see Subsection § 2.2.2). However, in the following we present a derivation of the mesh velocity field in the Monge-Kantorovich mass transfer problem framework. To this end, fix a time interval [0, T], and without loss of generality, set T=1. To generate an adaptive mesh define a transformation $\boldsymbol{x} : \Omega_c \rightarrow \Omega$, $\boldsymbol{x} = \boldsymbol{x}(\boldsymbol{\xi}, t)$. Suppose that the density function $\rho(\boldsymbol{x}, t) > 0$, $t \in [0, 1]$ is given. Let $\boldsymbol{x}_t := \boldsymbol{v}$ be the mesh velocity field, which satisfy the conservation of mass equation

$$\frac{\partial \rho}{\partial t} + \nabla \cdot (\rho \boldsymbol{v}) = 0 \tag{3.9}$$

and the boundary condition

$$\boldsymbol{v} \cdot \mathbf{n} = 0, \tag{3.10}$$

where $\mathbf{n}$ is the outward unit vector normal to the $\partial\Omega$.

The energy of the transformation can be defined as

$$E(\boldsymbol{v}) = \int_0^1 \int_\Omega \frac{1}{2}\rho(\boldsymbol{x}, t)\left|\boldsymbol{v}(\boldsymbol{x}, t)\right|^2 \, d\boldsymbol{x}dt. \tag{3.11}$$

We can link the co-ordinate transformation defined for the GCL method to the optimal mapping defined for the MKP via the following theorem.

**Theorem 3.1.** The mesh velocity field $\boldsymbol{x}_t = \boldsymbol{v}$ in the GCL method [1] can be determined as a minimizer of the energy (3.11), subject to the conditions (3.9) and (3.10), and the obtained velocity field has the form

$$\boldsymbol{v}(\boldsymbol{x}, t) = \nabla\phi(\boldsymbol{x}, t), \tag{3.12}$$

where the potential function $\phi$ is the Lagrange multiplier of the constraint (3.9).

**Proof 3.1.** The Lagrangian for this minimization problem is defined as

$$L(\boldsymbol{v}, \phi) = \int_0^1 \int_\Omega \left\{ \frac{1}{2}\rho |\boldsymbol{v}|^2 + \phi \left( \frac{\partial \rho}{\partial t} + \nabla \cdot (\rho \boldsymbol{v}) \right) \right\} d\boldsymbol{x}dt. \tag{3.13}$$

The minimum of the functional (3.13) occurs when

$$\frac{\partial L}{\partial \phi} = 0, \ \frac{\partial L}{\partial \boldsymbol{v}} = 0. \tag{3.14}$$

If $\frac{\partial L}{\partial \phi} = 0$, then differentiating (3.13) with respect to $\phi$ yields

$$\int_0^1 \int_\Omega \left( \frac{\partial \rho}{\partial t} + \nabla \cdot (\rho \boldsymbol{v}) \right) d\boldsymbol{x}dt = 0, \tag{3.15}$$

and since the spatial and time domains of integrations are chosen arbitrarily, (3.15) gives the continuity equation (3.9). To show (3.12), consider

$$\nabla \cdot (\phi\rho\boldsymbol{v}) = \nabla\phi \cdot (\rho\boldsymbol{v}) + \phi\nabla \cdot (\rho\boldsymbol{v}),$$

or equivalently

$$\phi\nabla \cdot (\rho\boldsymbol{v}) = \nabla \cdot (\phi\rho\boldsymbol{v}) - \nabla\phi \cdot (\rho\boldsymbol{v}).$$

This gives,

$$\int_\Omega \phi\nabla \cdot (\rho\boldsymbol{v})\, d\boldsymbol{x} = \int_\Omega \nabla \cdot (\phi\rho\boldsymbol{v})\, d\boldsymbol{x} - \int_\Omega \nabla\phi \cdot (\rho\boldsymbol{v})\, d\boldsymbol{x}, \tag{3.16}$$

and by using the divergence theorem we obtain

$$\int_\Omega \nabla \cdot (\phi\rho\boldsymbol{v})\, d\boldsymbol{x} = \int_{\partial\Omega} \phi\rho\boldsymbol{v} \cdot \mathbf{n}\, dS,$$

where $\mathbf{n}$ is the outward unit vector normal to $\partial\Omega$. Using (3.10) we get

$$\int_\Omega \nabla \cdot (\phi\rho\boldsymbol{v})\, d\boldsymbol{x} = \int_{\partial\Omega} \phi\rho\boldsymbol{v} \cdot \mathbf{n}\, dS = 0. \tag{3.17}$$

Therefore, (3.16) reduces to

$$\int_{\Omega} \phi \nabla \cdot (\rho \boldsymbol{v})\, d\boldsymbol{x} = -\int_{\Omega} \nabla\phi \cdot (\rho \boldsymbol{v})\, d\boldsymbol{x}, \tag{3.18}$$

and $L(\boldsymbol{v}, \phi)$ becomes

$$L(\boldsymbol{v}, \phi) = \int_0^1 \int_{\Omega} \left\{ \frac{1}{2}\rho|\boldsymbol{v}|^2 + \phi\frac{\partial \rho}{\partial t} - \nabla\phi \cdot \rho\boldsymbol{v} \right\} d\boldsymbol{x}dt. \tag{3.19}$$

If $\frac{\partial L}{\partial \boldsymbol{v}} = 0$, then differentiating (3.19) with respect to $\boldsymbol{v}$ yields

$$\int_0^1 \int_{\Omega} (\rho\boldsymbol{v} - \rho\nabla\phi)\, d\boldsymbol{x}dt = 0. \tag{3.20}$$

Taking into account that the spatial and time domains of integrations are chosen arbitrarily, (3.20) gives

$$\rho\boldsymbol{v} - \rho\nabla\phi = 0, \text{ or equivalently } \boldsymbol{v} = \nabla\phi, \tag{3.21}$$

This shows that the velocity $\boldsymbol{v} = \nabla\phi$ minimizes the energy of the transformation.

□

Note that constraint (3.9) of the minimization problem in Theorem 3.1 is originally derived from the geometric conservation law (2.40) and the generalized form of the equidistribution principle (2.63) in the GCL method formulation [1]. In other words the constraint (3.9) has been derived as a result of the idea of adaptivity and the volume preserving law in the GCL method. This constraint has also been derived as a result of conservation of mass in the optimal mass transport problem. Theorem 3.1 shows that the mesh velocity field (3.12) that minimizes the transportation energy (3.11) is a gradient of the potential $\phi$; therefore, it is a curl free vector field. i.e., $\nabla \times \boldsymbol{v} = \boldsymbol{0}$. This means that the velocity field is free of rotation and the corresponding transformation can be thought of the nearest transformation to the identity. This result agrees with the result obtained by Cao, Huang and Russell [1]. In fact, the velocity (3.12) obtained in the MKP framework is a particular case of the velocity (2.54) derived in [1] when $\mathbf{u} = \mathbf{0}$ and $w = 1$.

Substituting (3.12) into (3.9) and (3.10) yields

$$\nabla \cdot (\rho \nabla \phi) = -\frac{\partial \rho}{\partial t}, \tag{3.22}$$

and

$$\nabla \phi \cdot \mathbf{n} = 0 \text{ on } \partial\Omega. \tag{3.23}$$

Solving (3.22) and (3.23) for $\phi$, then the optimal mapping, or equivalently the adaptive mesh for a given initial mesh $\boldsymbol{x}(\boldsymbol{\xi}, 0) = \boldsymbol{\xi}$, can be computed by integrating

$$\boldsymbol{x}_t = \nabla \phi(\boldsymbol{x}, t). \tag{3.24}$$

## 3.2 Links with Fluid Dynamics

In this section we show some links between the transformation techniques of moving mesh methods and those found in fluid dynamics.

In the literature of fluid dynamics, we have the Reynolds transport theorem,

$$\frac{d}{dt}\int_{\Omega(t)} F(\boldsymbol{x}, t)\, d\boldsymbol{x} = \int_{\Omega(t)} \frac{\partial F}{\partial t}\, d\boldsymbol{x} + \int_{\partial\Omega} F\boldsymbol{v} \cdot \mathbf{n} dS, \tag{3.25}$$

where $F(\boldsymbol{x}, t)$ represents a property of the fluid, $\mathbf{n}$ is a unit vector normal to $\partial\Omega$ and $\Omega(t)$ is the fluid volume.

For $F(\boldsymbol{x}, t) = 1$, the Reynolds transport theorem reduces to

$$\frac{d}{dt}\int_{\Omega(t)} d\boldsymbol{x} = \int_{\partial\Omega} \boldsymbol{v} \cdot \mathbf{n} dS. \tag{3.26}$$

This is precisely the geometric conservation law that has been used in the derivation of the GCL method (see Subsection § 2.2.2). Also, for $F(\boldsymbol{x}, t) = \rho$ (the fluid density), and using the divergence theorem the Reynolds transport theorem gives the conservation of mass equation

$$\frac{\partial \rho}{\partial t} + \nabla \cdot (\rho \boldsymbol{v}) = 0. \tag{3.27}$$

Note that this is just the moving mesh equation derived earlier in the GCL method formulation (see Section § 2.2.2).

Solving the incompressible fluid dynamics problems in Lagrangian co-ordinates reduces to solving the Lagrangian system (see [45])

$$\boldsymbol{x}_t = \mathbf{u}_f(\boldsymbol{x}(t), t)\ \boldsymbol{x}(0) = \boldsymbol{x}_0 \tag{3.28}$$

where $\mathbf{u}_f$ is the flow velocity field. From moving mesh theory we know that most of the moving mesh methods are based on a Lagrangian type approach which is best introduced via a co-ordinate transformation. The fluid flow equation (3.28) can be considered as a moving mesh equation, where the fluid particles are treated as mesh points. In fact in [1] it is shown that the GCL method can be considered as a generalization of the Lagrangian method when choosing the background velocity $\boldsymbol{u}$ to be the flow velocity $\boldsymbol{u}_f$.This can be shown by recalling the system (see Subsection § 2.2.2)

$$\boldsymbol{x}_t = \mathbf{u}(\boldsymbol{x}, t) + \frac{1}{w}\nabla\phi(\boldsymbol{x}, t) \text{ in } \Omega, \tag{3.29a}$$

$$\nabla \cdot \left(\frac{\rho}{w}\nabla\phi\right) = -\frac{\partial\rho}{\partial t} - \nabla \cdot (\rho\mathbf{u}) \text{ in } \Omega, \tag{3.29b}$$

$$\frac{\partial\phi}{\partial n} = -w\mathbf{u} \cdot \mathbf{n} \text{ on } \partial\Omega, \tag{3.29c}$$

and considering the case $\rho$ is constant for incompressible fluid flow, where from $\nabla \cdot \mathbf{u}_f = 0$ (conservation of mass equation (3.9)) we have $\phi =$ constant. Hence, for $w = 1$ (3.29a) reduces to (3.28).

## 3.3 Links with Semi-geostrophic Equations

In [33] Budd and Piggot present a link between the analytical transformation found in solving the semi-geostrophic equations in meteorology and the adaptivity ideas. In this section we present their findings for the one-dimensional problem, but for the two- and three-dimensional problems we show this link in a different way than that given by Budd and Piggot.

Recall that in Section § 2.4 a co-ordinate transformation from a physical domain $(x, y, z)$ to a dual space (X,Y,Z),

$$\boldsymbol{X} \equiv (X, Y, Z)^T = \left(x + \frac{v_g}{f}, y - \frac{u_g}{f}, \frac{g\theta}{f^2\theta_0}\right)^T, \tag{3.30}$$

is defined to solve the semi-geostrophic equations (2.76a, 2.76b, 2.76c). Since the dual space is where the computations are performed, then the transformation (3.30) can be thought of as a transformation from a physical domain $\Omega$ to a computational domain $\Omega_c$.

Transformation (3.30) describes the evolution of the spatial mesh. Under this transformation the semi-geostrophic equations (2.76a, 2.76b, 2.76c) were shown to take the form [38], [34], [33] (see Section § 2.4)

$$\frac{D\boldsymbol{X}}{Dt} = \mathbf{u}_g \equiv (u_g, v_g, 0)^T, \tag{3.31}$$

In the previous section, it is shown that the GCL method can be considered as a generalization of the Lagrangian method. Thus, a numerical method based on (3.31) will perform in an adaptive way, and is a Lagrangian form of mesh adaptivity where the mesh moves at the speed of the wind velocity field.

In Section § 2.4, the Jacobian of the transformation (3.30) is shown to be written as

$$q = \frac{\partial(X, Y, Z)}{\partial(x, y, z)} = \det(H_x(P)). \tag{3.32}$$

Now we show a relationship between the transformation (3.30) and the transformational techniques of mesh adaptivity.

In one-dimensional space, we have the equidistribution principle

$$\frac{\partial x}{\partial \xi} = \frac{1}{M}.$$

If we take the monitor function $M = q$ in (3.32), and set the computational variable $X$ to be $\xi$ then (3.32) reduces to

$$M = P_{xx}.$$

This equation shows a relationship between the transformation defined for solving the semi-geostrophic equations and the monitor function introduced for the mesh adaption in moving mesh methods.

In three-dimension, Budd and Piggott use the co-ordinate transformation techniques defined in [22] to establish a link between the transformation defined in (3.30) and the idea of the mesh adaptivity. We now proceed by a different route and show

this link via the co-ordinate transformation defined for the GCL method [1]. To this end, recall from the GCL method in Section §2.2.2 that we have the generalization of the equidistribution principle relation

$$J(\boldsymbol{\xi}, t) = \frac{\partial \boldsymbol{x}}{\partial \boldsymbol{\xi}} = \frac{c(\boldsymbol{\xi})}{\rho(\boldsymbol{x}(\boldsymbol{\xi}), t)}. \tag{3.34}$$

Comparing (3.32) and (3.34), if we take $c(\boldsymbol{\xi}) = 1$ and $\rho = q$, then (3.32) reduces to

$$\rho = \det(H_x(P));$$

thus, the geostrophic equations can be solved if the density $\rho$ is found. Therefore, we have shown some link between the co-ordinate transformation found in the literature of semi-geostrophic equations in meteorology and the mesh adaptivity techniques used in moving mesh methods.

## 3.4 Links with Computational Anatomy

The comparison between two manifolds (e.g., points, curves, surfaces and submanifolds) in computational anatomy is based on co-ordinate transformations between these manifolds. In this section, we show a relationship between the co-ordinate transformations between these manifolds and mesh adaptivity techniques for moving mesh methods. To this end, recall that in computational anatomy (see Section § 2.5) we have the system of equations

$$\frac{\partial}{\partial t}\boldsymbol{x}(\boldsymbol{\xi}, t) = \boldsymbol{v}(\boldsymbol{x}(\boldsymbol{\xi}, t), t), \tag{3.35a}$$

$$\frac{\partial}{\partial t}\boldsymbol{\xi}(\boldsymbol{x}, t) = -D\boldsymbol{\xi}(\mathbf{x}, \mathbf{t})\boldsymbol{v}(\boldsymbol{x}, t), \tag{3.35b}$$

$$\boldsymbol{x}(0) = \boldsymbol{\xi}(0) = \mathrm{id}, \tag{3.35c}$$

describing the transformations as arising from an evolution in time. In moving mesh terminology, the solutions of the system (3.35) can be thought of as co-ordinate transformations between a computational domain $\Omega_c$ and a physical domain $\Omega$, where $\boldsymbol{\xi}$ and $\boldsymbol{x}$ are the computational and physical variables respectively. The evolution equations are in Lagrangian form. Therefore, by the discussion given in Section § 3.3, the system (3.35) can be considered as a particular case of the GCL method [1].

In Section § 2.5 it is shown that the problem of CA is to determine the shortest length curve $\boldsymbol{x}(t)$, $t \in [0,1]$ which minimizes the target norm $\|\mathrm{I}_0(\boldsymbol{\xi}(1)) - \mathrm{I}_1\|^2$. In other words, the goal in CA is to find an optimal mapping that transfers $\mathrm{I}_0$ to $\mathrm{I}_1$ and minimizes the distance between the two images. In moving mesh methods terminology, this is equivalent to finding a co-ordinate transformation between a computational domain and a physical domain which is close to the identity. In Section § 2.5 it is also shown that the velocity field can be determined as the minimizer of

$$\inf_{\boldsymbol{x}} \int_0^1 E_v(t)dt = \inf_{\boldsymbol{x}} \int_0^1 \|\boldsymbol{v}(t)\|_L^2 dt, \tag{3.36}$$

where $\boldsymbol{x}$ satisfies the system (3.35).

In the GCL method framework it is shown that the mesh velocity can be determined by minimizing the functional (see Section § 3.1)

$$\int_0^1 \int_\Omega \frac{1}{2}\rho(\boldsymbol{x},t)\,|\boldsymbol{v}(\boldsymbol{x},t)|^2 \; d\boldsymbol{x}dt. \tag{3.37}$$

Thus we conclude that, for both the GCL method and computational anatomy formulations, the velocity field $\boldsymbol{v}$ is obtained by minimizing a transportation cost, and both have an inherent relation to the Lagrangian method.

## 3.5 Links with Image Registration

Recall that the image registration problem in Section § 2.5 is defined as a problem of constructing a co-ordinate transformation between two data sets.

To establish a link between transformations of data sets and the idea of mesh adaptivity in moving mesh methods, we state the following theorem found in the literature of image registration (see [30]).

**Theorem 3.2.** Suppose two images are taken at times $t_0$ and t respectively. The first one has density $\rho_0 > 0$, defined on $\Omega_0$, and the second one has density $\rho > 0$, defined on $\Omega$. If the two images are assumed to differ only as a result of the motion of particles in the three-dimensional scene, then there exists a one-to-one two-dimensional

mapping $\Psi : \mathbb{R}^2 \rightarrow \mathbb{R}^2$ that transforms points $\boldsymbol{\xi} \in \Omega_0$ into their corresponding points $\boldsymbol{x} = \Psi(\boldsymbol{\xi}) \in \Omega$. The associated change is given by

$$\rho(\boldsymbol{x}) = J_{\Psi}^{-1}(\boldsymbol{\xi})\rho_0(\boldsymbol{\xi}) \tag{3.38}$$

where $J_{\Psi}^{-1}$ is the inverse of the Jacobian of the mapping $\Psi$.

□

(3.38) implies that if a small region in $\Omega_0$ is mapped to larger region in $\Omega$, then there must be a corresponding decrease in density, which is the idea of the equidistribution principle. Recall that the GCL method in Section § 2.2.2 has the following form for mesh adaptation:

$$J = \frac{c(\boldsymbol{\xi})}{\rho(\boldsymbol{x})}. \tag{3.39}$$

If we consider the first image domain $\Omega_0$ as a computational domain and the target image domain $\Omega$ as a physical domain. then by taking $\rho_0(\boldsymbol{\xi}) = c(\boldsymbol{\xi})$, (3.38) will be the same as the GCL method relation (3.39). Hence we see that there is a link between the co-ordinate transformations used in the image registration process and the adaptivity technique for the GCL method.

# Chapter 4

# Numerical Experiments

In Section § 3.1 (see theorem 3.1), it is shown that the mesh velocity field can be derived by minimizing the energy of the transformation which is shown to be a curl free vector field $\boldsymbol{v} = \nabla\phi$. This curl free vector field is shown to be a particular case of the velocity field derived for the GCL method. To understand different features of the GCL method and to explain how the adaptive mesh computed by the GCL method can be interpreted as a mapping that solves the Monge-Kantorovich mass transfer problem, in this chapter we use the velocity form $\boldsymbol{v} = \nabla\phi$ to generate an adaptive mesh in two-dimensional space for which the density function is given. Precisely speaking, we solve the system

$$\boldsymbol{x}_t = \nabla\phi, \quad \text{in } \Omega \tag{4.1a}$$

$$\nabla \cdot \left(\frac{\rho}{w}\nabla\phi\right) = -\frac{\partial\rho}{\partial t}, \quad \text{in } \Omega \tag{4.1b}$$

$$\nabla\phi \cdot \mathbf{n} = 0, \quad \text{on } \partial\Omega \tag{4.1c}$$

to generate the adaptive mesh. The system (4.1) is defined on the physical domain $\Omega$. However, in order to perform the computations, we transform (4.1) to a computational domain $\Omega_c$. The system (4.1) can be rewritten in terms of the computational variables

$\boldsymbol{\xi} = (\xi, \eta)$ as follows (see [39]):

$$\frac{\partial \boldsymbol{x}}{\partial t} = \mathrm{J}^{-1} C^T \nabla_c \phi, \tag{4.2a}$$

$$\mathrm{J}^{-1} \nabla_c \cdot (A \nabla_c \phi) = -\frac{\partial \rho}{\partial t} + \mathrm{J}^{-1} \dot{\boldsymbol{x}} \cdot C^T \nabla_c \rho, \tag{4.2b}$$

$$\mathrm{J}^{-1} C \nabla_c \phi \cdot \mathbf{n} = 0, \tag{4.2c}$$

where

$$C = \begin{bmatrix} y_\eta & -y_\xi \\ -x_\eta & x_\xi \end{bmatrix},$$

$\nabla_c$ is a spatial gradient operator defined on $\Omega_c$ as

$$\nabla_c = \left( \frac{\partial}{\partial \xi}, \frac{\partial}{\partial \eta} \right)^T,$$

J is defined as

$$\mathrm{J} = \begin{vmatrix} x_\xi & x_\eta \\ y_\xi & y_\eta \end{vmatrix} = x_\xi y_\eta - x_\eta y_\xi,$$

and

$$A = J^{-1} C^T \rho C = \begin{bmatrix} a^{11} & a^{12} \\ a^{21} & a^{22} \end{bmatrix},$$

where

$$a_{11} = \frac{\rho}{\mathrm{J}} \left( x_\eta^2 + y_\eta^2 \right), \; a_{12} = a_{21} = -\frac{\rho}{\mathrm{J}} \left( x_\xi x_\eta + y_\xi y_\eta \right) \text{ and } a_{22} = \frac{\rho}{\mathrm{J}} \left( x_\xi^2 + y_\xi^2 \right).$$

## 4.1 Finite Difference Scheme

In this section, we show how the system (4.2) can be discretized and transformed into a linear system of difference equations.

For spatial and temporal discretization of the system (4.2), let

$$h = \frac{1}{N}, \boldsymbol{\xi}_{ij} = (ih, jh), \Delta t > 0, t^n = n\Delta t, \text{ and } w(\boldsymbol{\xi}_{ij}, t^n) = w_{ij}^n.$$

Now, let $\boldsymbol{x}_{ij}^n$ and $o_{ij}^n$ denote approximations at time $t^n$. These values may be used for the spatial discretization of (4.2b) and (4.2c) by using a standard finite difference

method on a nine point stencil (see figure 4.1). As a result of this discretization we obtain a linear system of algebraic equations in $\phi_{ij}^{n+1}$. Approximations $\phi_{ij}^{n+1}$ can be obtained by solving the resulting linear system. The new mesh at $t^{n+1}$ may be obtained by discretizing (4.2a), first in the spatial domain by using the standard centered finite difference to obtain a system of ODEs and then discretizing the resulting ODEs system in time using a suitable finite difference method.

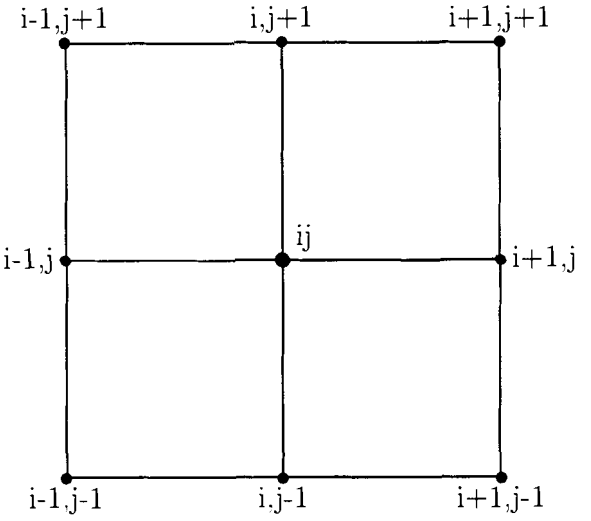


Figure 4.1: The nine stencil used in discretization in the spatial domain

To find a corresponding system of difference equations to the system (4.2), replace the terms $J$ and $\nabla_c$ by the finite difference terms

$$J_{ij}^n = [\delta_\xi x \delta_\eta y - \delta_\eta x \delta_\xi y]_{ij}^n$$

and

$$\tilde{\nabla}_h = \left[(\delta_\xi, \delta_\eta)^T\right]_{ij}^n.$$

For any function $g(\boldsymbol{x}, t)$ let

$$G_{i+1/2,j}^n = \frac{1}{2}[g(\boldsymbol{\xi}_{ij}, t^n) + g(\boldsymbol{\xi}_{i+1,j}, t^n)],$$

and define $G^n_{i,j+1/2}$ similarly. Let

$$\delta_{\bar{\xi}} \left(G\delta_\xi \phi\right)^n_{ij} = h^{-2} \left[G^n_{i+1/2,j} \left(\phi^n_{i+1,j} - \phi^n_{ij}\right) - G^n_{i-1/2,j} \left(\phi^n_{ij} - \phi^n_{i-1,j}\right)\right].$$

Then the term $\nabla_c \cdot A\nabla_c \phi$ can be approximated by

$$\begin{aligned}\tilde{\nabla}_h \left(A(\boldsymbol{x}^n_{ij})\tilde{\nabla}_h \phi\right)^{n+1}_{ij} &= \left[\delta_{\bar{\xi}} \left(A^{11}\delta_\xi \phi\right) + \delta_{\bar{\eta}} \left(A^{22}\delta_\eta \phi\right)\right]^{n+1}_{ij} + \\ &\quad \frac{1}{4}\left[\left(\delta_\xi + \delta_{\bar{\xi}}\right)\left(A^{12}\left(\delta_\eta + \delta_{\bar{\eta}}\right)\phi\right) + \left(\delta_\eta + \delta_{\bar{\eta}}\right)\left(A^{21}\left(\delta_\xi + \delta_{\bar{\xi}}\right)\phi\right)\right]^n_{ij},\end{aligned}$$

where $\delta_\xi$, $\delta_{\bar{\xi}}$, $\delta_\eta$, and $\delta_{\bar{\eta}}$ are the forward and backward difference quotients in the variables $\xi$ and $\eta$, and $A^{11}$, $A^{12} = A^{21}$, and $A^{22}$ are approximations of $a_{11}, a_{12} = a_{21}$ and $a_{22}$ evaluated at $\boldsymbol{x}^n$ and $t^n$. Therefore, (4.2b) and (4.2c) can be replaced by the difference equations

$$\left[\mathrm{J}^{-1}\right]^n_{ij} \left[\tilde{\nabla}_h \left(A(\boldsymbol{x}^n_{ij})\tilde{\nabla}_h \phi\right)\right]^{n+1}_{ij} = \left[-\frac{\partial \rho}{\partial t} + \mathrm{J}^{-1}\dot{\boldsymbol{x}} \cdot C^T \tilde{\nabla}_h \rho\right]^n_{ij}, \tag{4.3a}$$

$$\left[\mathrm{J}^{-1} C \tilde{\nabla}_h \phi \cdot \mathbf{n}\right]^n_{ij} = 0, \tag{4.3b}$$

and (4.2a) will be replaced by the ODEs system

$$\left[\frac{\partial \boldsymbol{x}}{\partial t}\right]^n_{ij} = \left[\mathrm{J}^{-1} C^T \tilde{\nabla}_h \phi\right]^n_{ij} := f^n_{ij}. \tag{4.4}$$

If the density function $\rho$ is given, then the system (4.3) is linear and can be rewritten in matrix form as

$$A\Phi = b. \tag{4.5}$$

To compute the new mesh $\boldsymbol{x}^{n+1}_{ij}$ at $t^{n+1}$, we solve the system (4.4) by using a 4th-order Runge-Kutta method.

For a given initial mesh $\boldsymbol{x}^0_{ij}$ and initial potential $\phi^0_{ij}$, the following procedure may be used to calculate the new mesh $\boldsymbol{x}^{n+1}_{ij}$:

1. Given approximations $\boldsymbol{x}^n$ and $\phi^n$ at time $t = t^n$, compute

$$K_1 = \Delta t f\left(t^n, \boldsymbol{x}^n_{ij}\right)$$

2. From (4.5) compute $\phi^{n+\frac{1}{2}}\left(\boldsymbol{x}^n_{ij} + \frac{1}{2}K_1\right)$

3. Calculate
$$K_2 = \Delta t f\left(t^{n+\frac{1}{2}}, \boldsymbol{x}_{ij}^n + \frac{1}{2}K_1\right)$$

4. From (4.5) compute $\phi_{ij}^{n+\frac{1}{2}}\left(\boldsymbol{x}_{ij}^n + \frac{1}{2}K_2\right)$,

5. Compute
$$K_3 = \Delta t f\left(t^{n+\frac{1}{2}}, \boldsymbol{x}_{ij}^n + \frac{1}{2}K_2\right)$$

6. From (4.5) compute $\phi_{ij}^{n+\frac{1}{2}}\left(\boldsymbol{x}_{ij}^n + K_3\right)$,

7. Compute
$$K_4 = \Delta t f\left(t^{n+\frac{1}{2}}, \boldsymbol{x}_{ij}^n + K_3\right)$$

8. Compute $\boldsymbol{x}_{ij}^{n+1}$ by setting
$$\boldsymbol{x}_{ij}^{n+1} = \boldsymbol{x}_{ij}^n + \frac{1}{6}\left(K_1 + 2K_2 + 2K_3 + K_4\right)$$

9. Set $n = n + 1$

10. Go to 1.

## 4.2 Numerical examples

In this section, we give some numerical examples of generating adaptive meshes in two-dimensional space for some given density functions.

In all of our numerical examples we choose $\Omega_c = \Omega = (0,1) \times (0,1)$, $\Omega_c$ to be a fixed $41 \times 41$ uniform rectangular mesh, and take a $41 \times 41$ uniform rectangular mesh as an initial mesh.

The choice of the density function is motivated by the fact that $\rho$ satisfies the generalized form of the equidistribution principle (2.41), so that $\rho$ can be interpreted as a density function, i.e., the computed mesh by $\rho$ is concentrated in regions where $\rho$ is large.

In order to satisfy the compatibility condition (2.52), we normalized the given density function at each step time. The function

$$E(\boldsymbol{x}, t) = \rho(\boldsymbol{x}, t)\mathrm{J}(\boldsymbol{x}, t),$$

is defined to show how accurate the computed mesh satisfies the equidistribution relation (2.41). The computed mesh is accurate when the function $E$ is close to 1.

For all of the examples, the density functions chosen to generate the mesh are similar to those used in [1].

**Example 4.1.** For the first example, an adaptive mesh will be generated by using the density function

$$\rho(\boldsymbol{x}) = 1 + A\exp\left(-50\,\left|(x-0.5)^2 + (y-0.5)^2 - 0.09\right|\right),$$

where A is a parameter adjusting the ratio of the largest cell size to the smallest one.

Using the GCL method the time-dependent density function can be defined as

$$\rho(\boldsymbol{x}, t) = 1 + t\,A\exp\left(-50\,\left|(x-0.5)^2 + (y-0.5)^2 - 0.09\right|\right).$$

If we let the time variable take values from $t = 0$ to $t = 1$, then the density function $\rho$ varies from $\rho_0 = 1$ to $\rho_1 = 1 + A\exp\left(-50\,|(x-0.5)^2 + (y-0.5)^2 - 0.09|\right)$. This can be thought of as an example of the Monge-Kantorovich problem for transferring the density $\rho_0$ to the density $\rho_1$. The mapping that solves the MKP in this case corresponds to the adaptive mesh at time $t = 1$.

We use a time step $\Delta t = 0.1$. The plots for the computed mesh and the function $E$ at time $t = 1$ with two parameter values $A = 5, 10$, are shown in figure 4.2. Note that the computed mesh is concentrated in the region where $\rho$ is large, i.e., in the region near the circle $(x-0.5)^2 + (y-0.5)^2 = 0.3^2$, which agrees with the results derived in [1]. The values of the function $E$ are between 0.8087 and 1.2502 for $A = 5$, and between 0.6575 and 1.7933 for $A = 10$. This shows that the larger the parameter A, the larger the density $\rho$.

□

**Example 4.2.** For this example, the mesh is generated by using a density function defined as

$$\rho(\boldsymbol{x},t) = \begin{cases} 1 + 50\,(0.1+t)\exp\left(-50\,(y-0.5)^2\right), & \text{for } -0.1 < t < 0, \\ 1 + 5\exp\left(-50\,(y-0.5-0.25\,\sin(2\pi x)\,\sin(2\pi t))^2\right), & \text{for } t \geq 0. \end{cases}$$

Note that the values of the density function $\rho$ vary from an initial density $\rho_0 = 1$ at $t = -0.1$ to $\rho_1 = 5\exp\left(-50\,(y-0.5)^2\right)$ at $t = 1$, which shows a transfer of density $\rho$ from $\rho_0$ to $\rho_1$. Again, the mapping that solves the MKP corresponds to the adaptive mesh at $t = 1$.

We use $\Delta t = 0.0005$. Figure 4.3 shows the plots of the computed mesh at four different times $t = 0,\ 0.25,\ 0.75$ and 1. Note that the density function is periodic. The computed mesh plots at $t = 0$ and $t = 1$ appear to be the same. However, these two plots are not identically the same plots because of the discretization errors. As expected, the generated mesh is concentrated in regions where the density $\rho$ is large.

□

**Example 4.3.** For this example, an adaptive mesh will be generated for the density function

$$\rho(\boldsymbol{x},t) = 1 + A\exp\big(-50\big(y-0.5-0.25\,\sin(2\pi x)\big)^2\big).$$

The time-dependent density function can be defined as

$$\rho(\boldsymbol{x},t) = 1 + t\,A\exp\big(-50\big(y-0.5-0.25\,\sin(2\pi x)\big)^2\big).$$

For this density function, we can think of a transfer of density from $\rho_0 = 1$ at $t = 0$ to $\rho 1 = 1 + A\exp\big(-50\big(y-0.5-0.25\,\sin(2\pi x)\big)^2\big)$ at $t = 1$. We use $\Delta t = 0.05$, and choose two values for the parameter $A = 5, 10$. Figure 4.4 shows the plots of the computed mesh and the function $E$ at $t = 1$. Note that for this example, the given density function is not periodic in time but maintains a sine wave shape. Also, here the mesh is concentrated in regions where the density $\rho$ is large, and the concentration increases with the increase of the parameter $A$. The values of the function $E$ vary between 0.9416 and 1.0220 for $A = 5$ and between 0.8673 and 1.0310 for $A = 10$.

□

**Example 4.4.** In this example, an adaptive mesh is generated by a density function defined as

$$\rho(\boldsymbol{x},t)=\begin{cases}1+100\,(0.1+t)\exp\left(-50\,|(x-0.5)^2+(y-0.5)^2-0.09|\right), & -0.1\le t\le 0,\\ 1+10\exp\left(-50\,|(x-0.5-t)^2+(y-0.5)^2-0.09|\right), & t\ge 0.\end{cases}$$

The time step used for this example is $\Delta t = 0.01$. The plots for the computed mesh for this density function are shown in figure 4.5. Note that the mesh is also concentrated around the circle $(x-0.5)^2+(y-0.5)^2=0.3^2$ at time $t=0$ and the circle shape moves to the right till it leaves the domain.

□

**Example 4.5.** In example 4.3 above we notice that the computed mesh is concentrated around a circle moving to the right while time changes. It would be interesting to see mesh adaption which shows two circles moving in two opposite directions. In this example we show this picture by defining the following two densities:

$$\rho_1=\begin{cases}1+50\,(0.1+t)\exp\left(-50\,|(x-0.65)^2+(y-0.5)^2-0.09|\right), & -0.1\le t\le 0,\\ 1+5\exp\left(-50\,|(x-0.65-t)^2+(y-0.5)^2-0.09|\right), & t\ge 0,\end{cases}$$

$$\rho_2=\begin{cases}1+50\,(0.1+t)\exp\left(-50\,|(x-0.25)^2+(y-0.5)^2-0.09|\right), & -0.1\le t\le 0.\\ 1+5\exp\left(-50\,|(x-0.25-t)^2+(y-0.5)^2-0.09|\right), & t\ge 0,\end{cases}$$

The plots of the generated mesh and the function $E$ at different times are shown in figures 4.6, 4.7, 4.8 and 4.9, each of which shows that the computed mesh is concentrated around two circular regions. These two circles move as time evolves till they leave the domain while maintaining their circular shapes.

□

## 4.3 Remarks

In the above examples we have indicated that the computed adaptive mesh at time $t=1$ corresponds to the optimal mapping that solves the Monge-Kantorovich mass

transfer problem, i.e., the mapping that transfers $\rho_0$ to $\rho_1$ with minimum transportation energy. However, in solving the Monge-Kantorovich mass transfer problem the density in the time between the initial and final times is not given. It can be computed together with the velocity field by solving a set of Euler Lagrange equations obtained from minimizing an energy functional subjected to some constraints (see Section § 2.3). In fact, in moving mesh methods, when solving a physical problem the density function is computed from the physical solution. There is need to do a numerical study in greater detail to show how to use these transformational techniques for mesh adaption to solve the Monge-Kantorovich mass transfer problem. Recently, Budd and Williams [17] show some interesting numerical results generating adaptive meshes using the Monge-Ampere equation.

In example 4.1 and example 4.2, we use the procedure explained in the previous sections to compute the mesh, and the code we use in the computations of these two examples is written in Fortran. For example 4.3, example 4.4 and example 4.5, we follow the approach of Cao, Huang and Russell [1] in the computations of the adaptive mesh, and we use the GCL code which was originally written for the numerical experiments in [1].

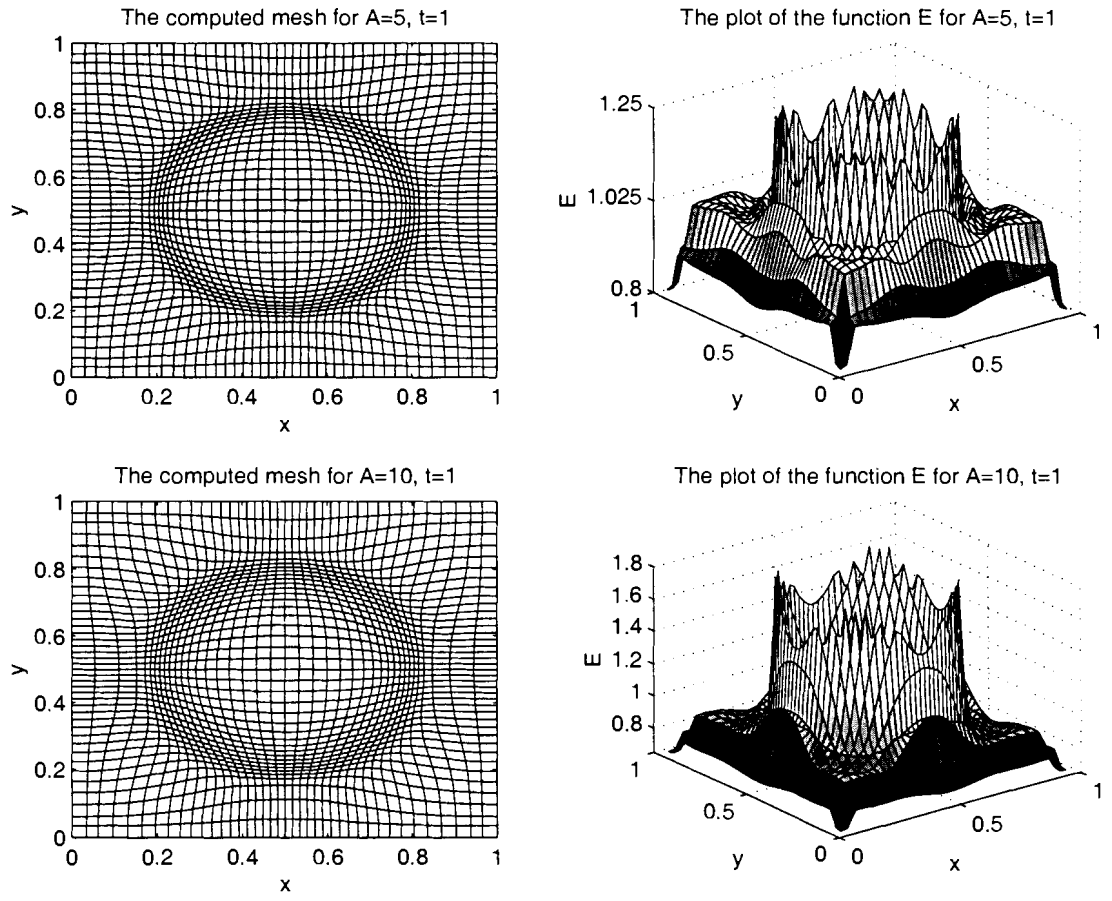


Figure 4.2: Example 4.1: The mesh solution at $t = 1$, for $A = 5$, 10.

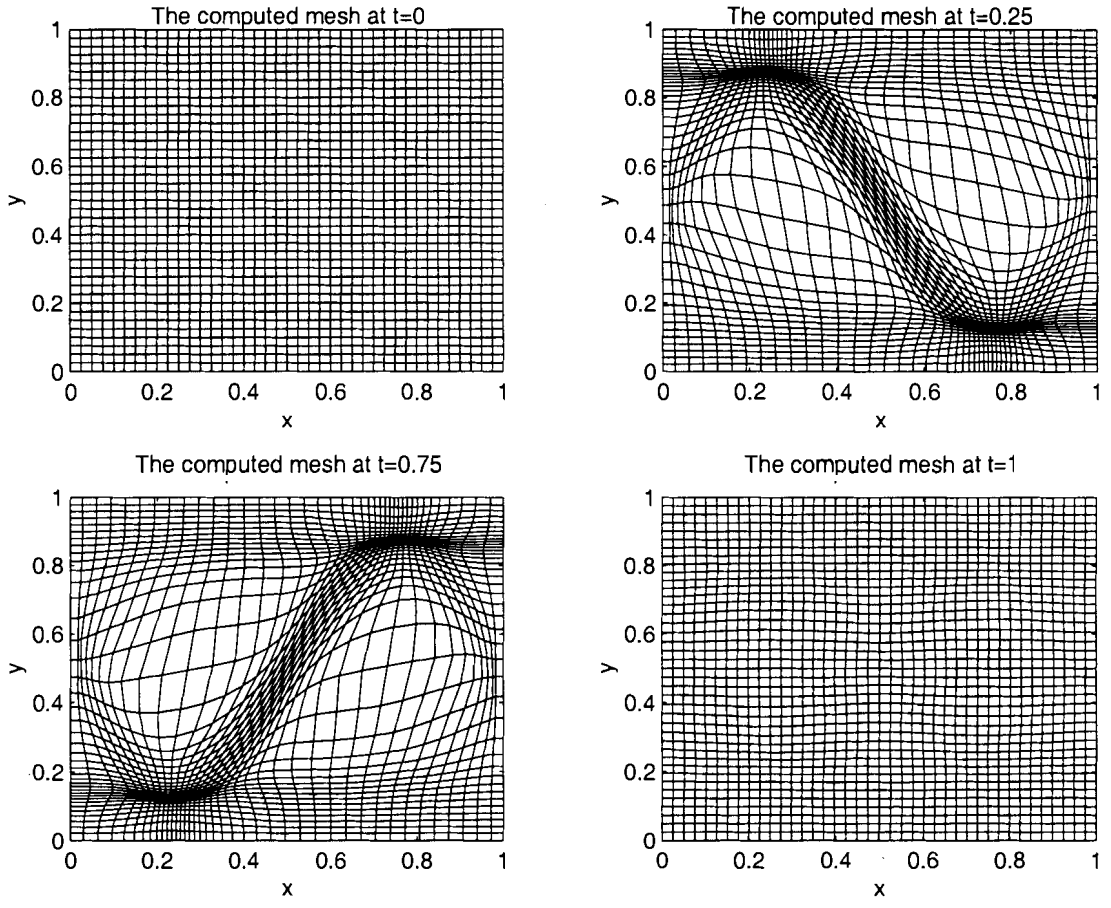


Figure 4.3: Example 4.2: The mesh solutions at $t = 0$, 0.25, 0.75, 1

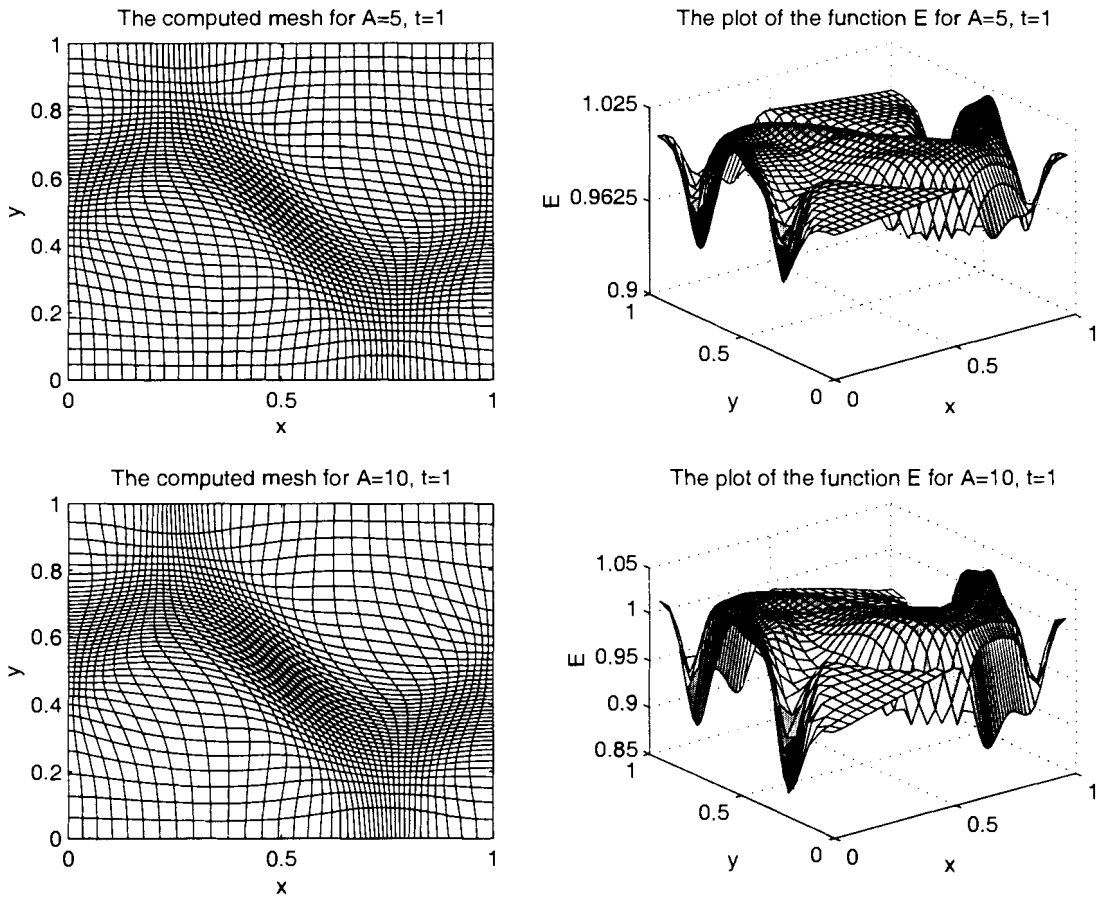


Figure 4.4: Example 4.3: The computed mesh and the function E at $t = 1$.

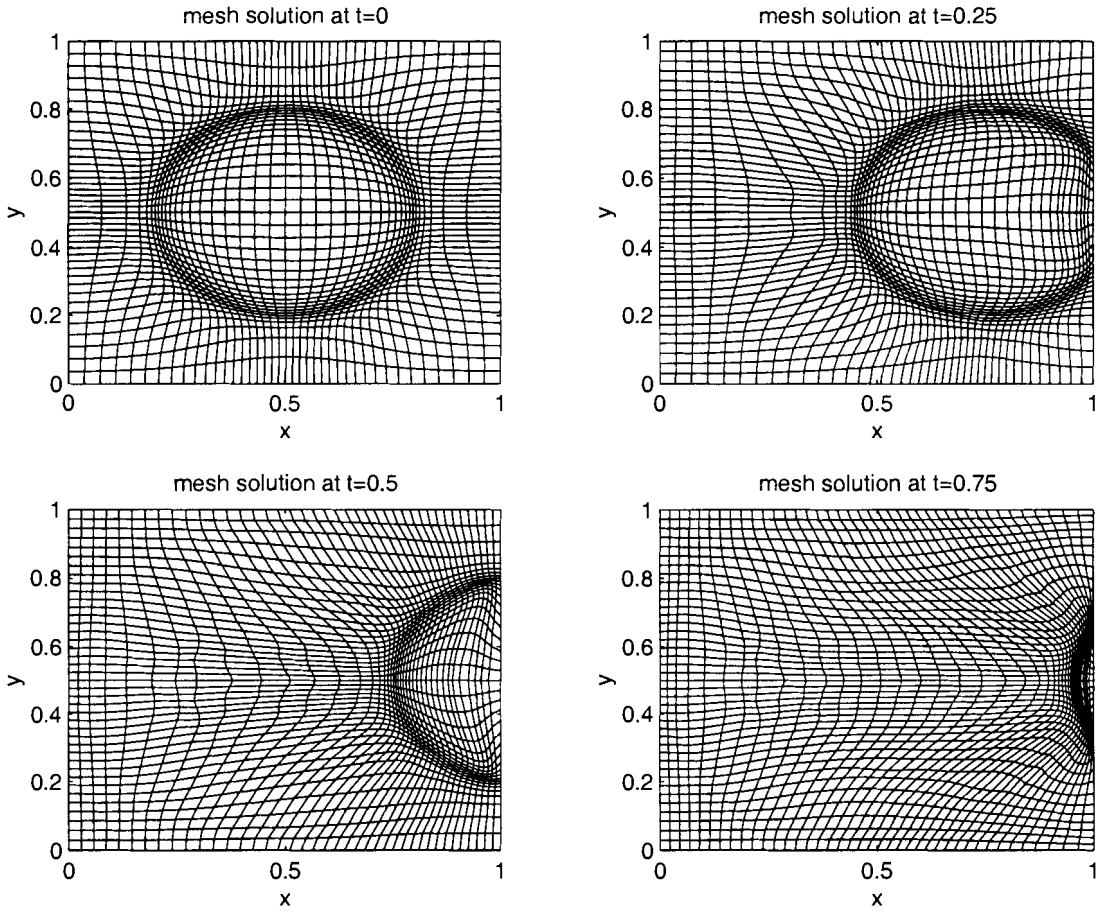


Figure 4.5: Example 4.4: The mesh solution at $t = 0, 0.25, 0.5, 0.75$.

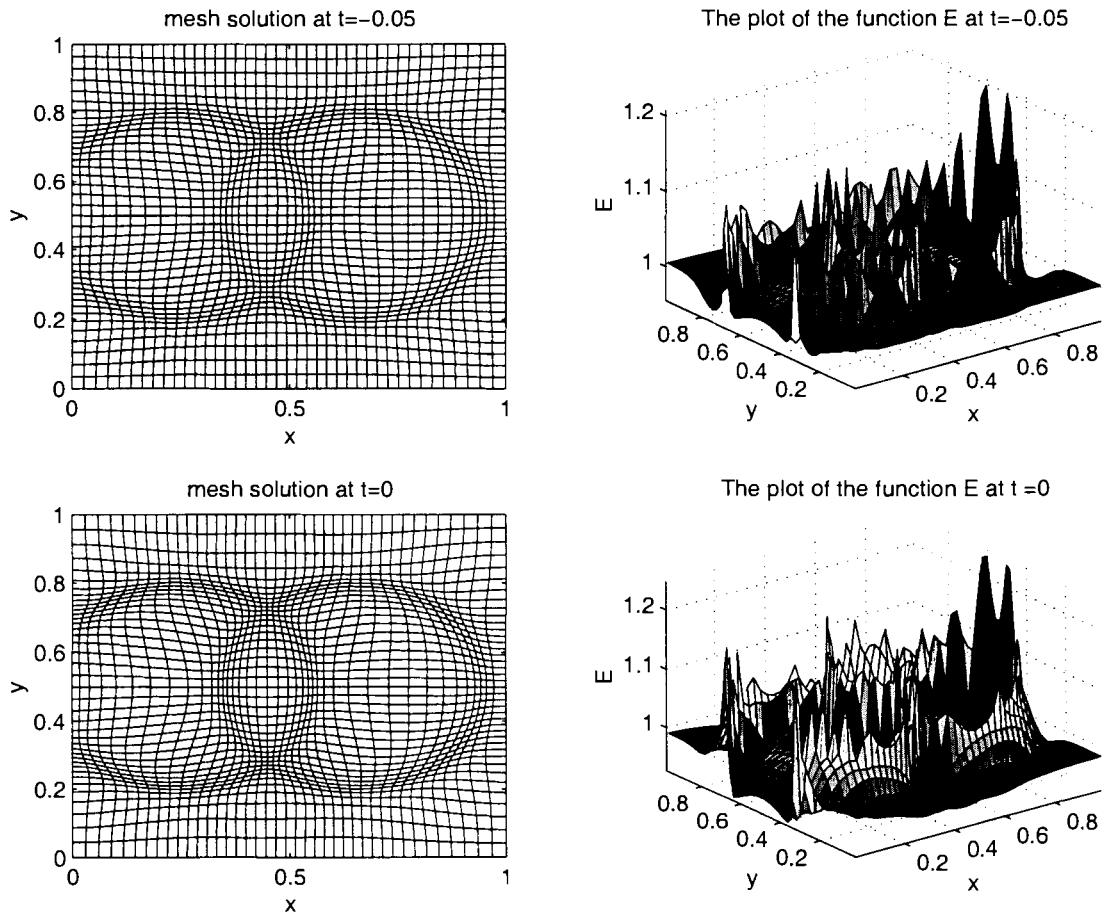


Figure 4.6: Example 4.5: The plot of the mesh and E at $t = -0.05$, 0.

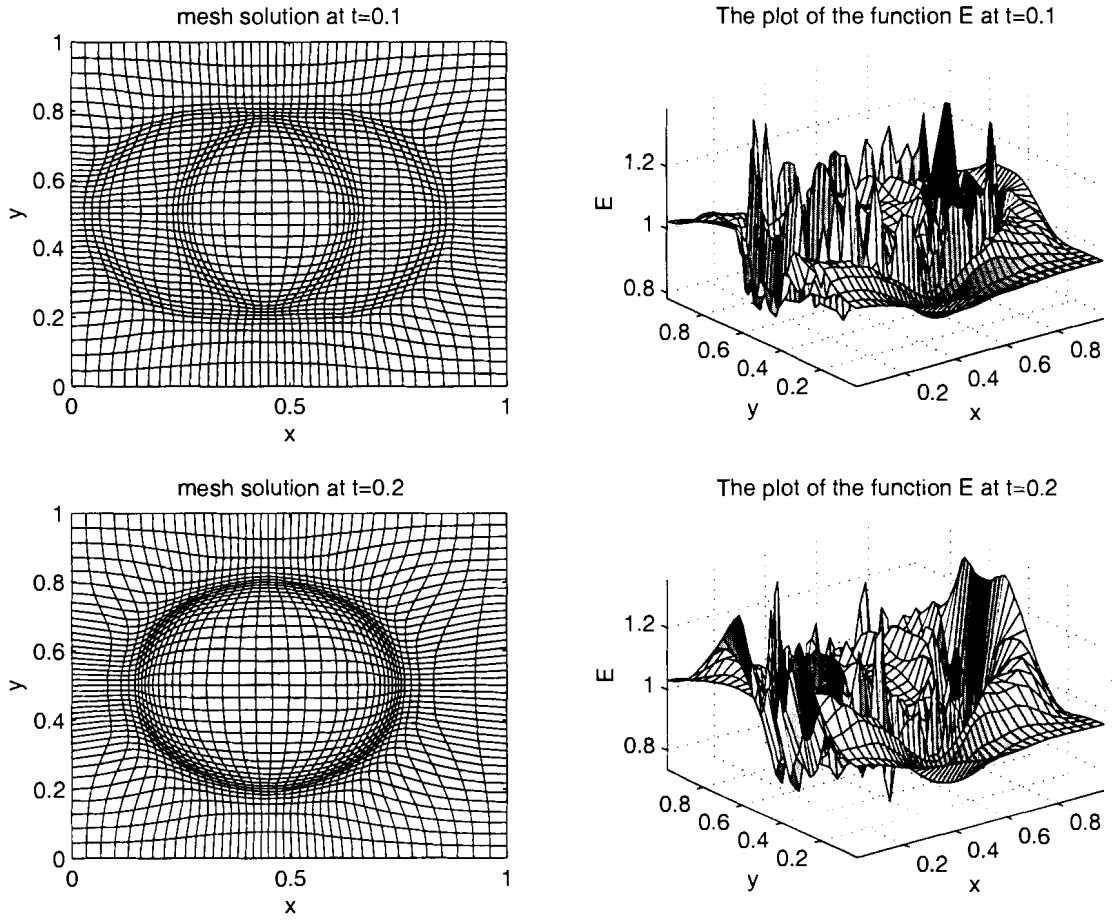


Figure 4.7: Example 4.5: The plot of the mesh and E at $t = 0.1, 0.2$.

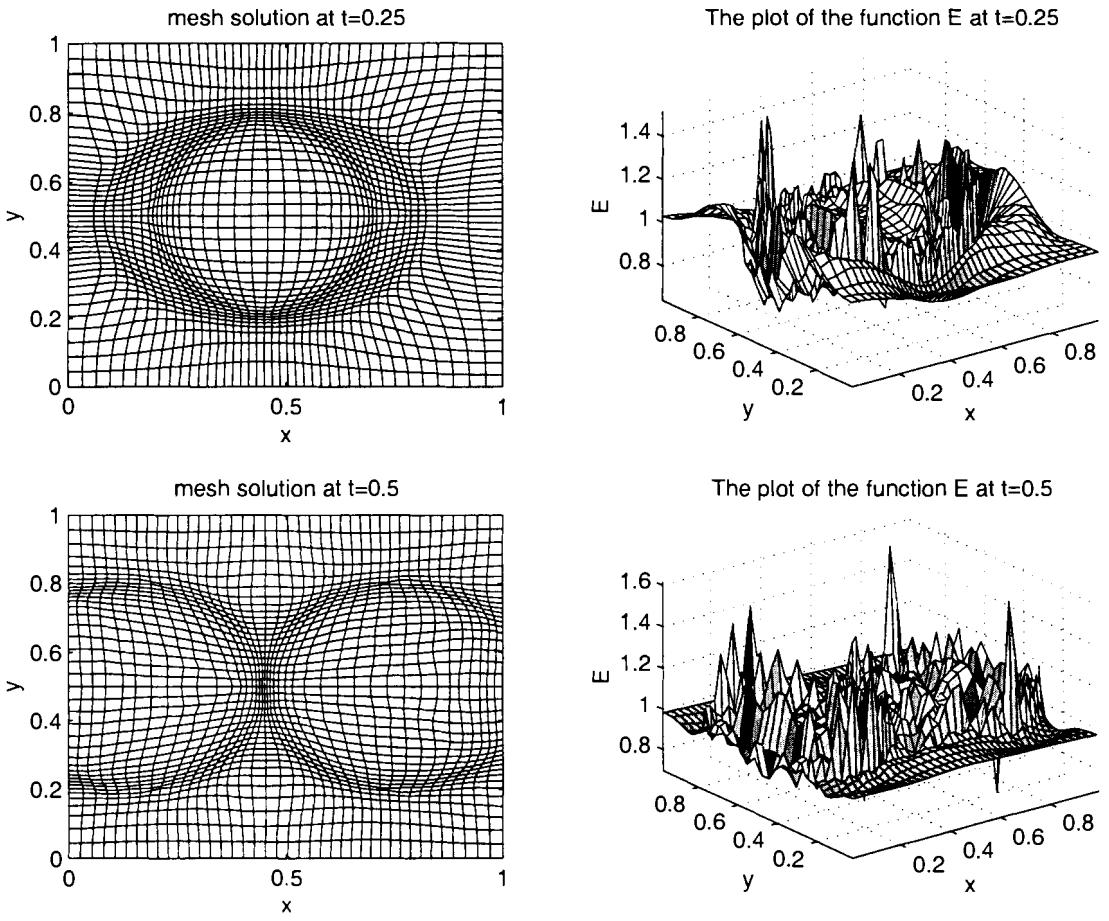


Figure 4.8: Example 4.5: The plot of the mesh and E at $t = 0.25, 0.5$.

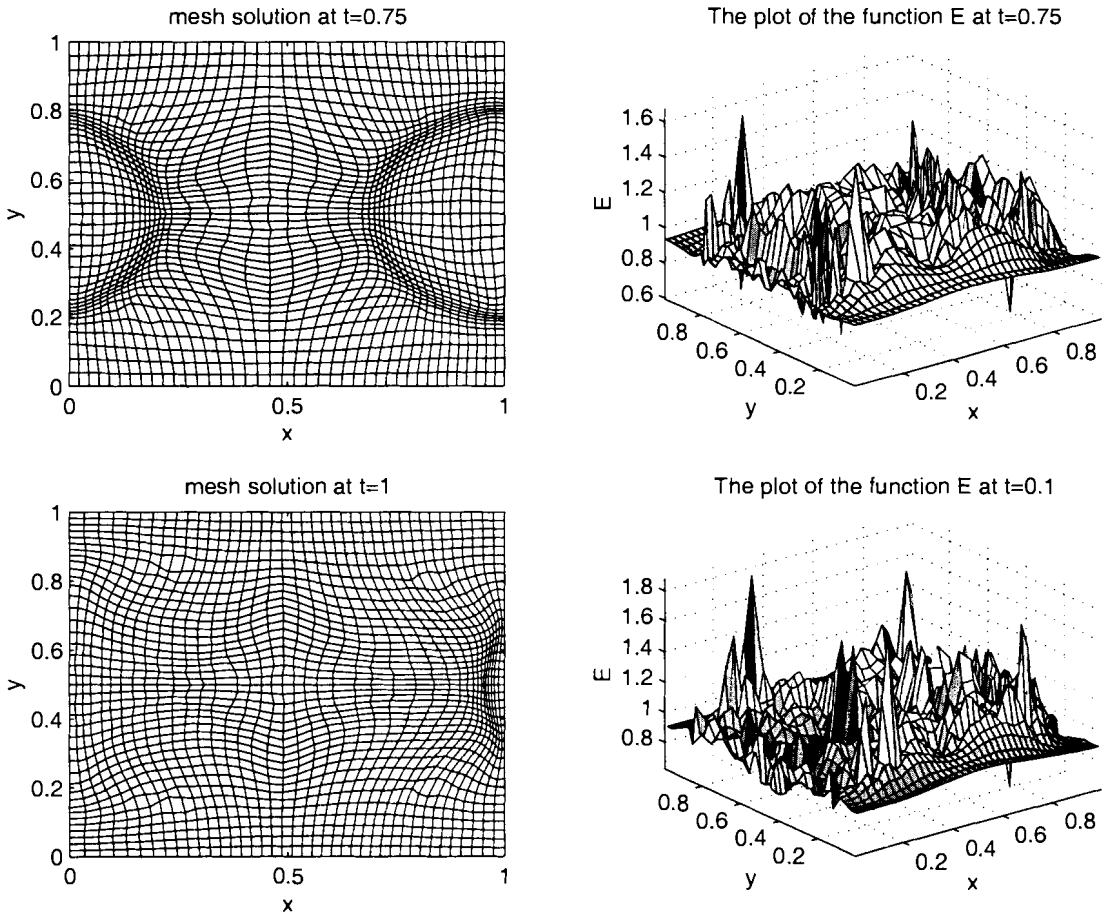


Figure 4.9: Example 4.5: The plot of the mesh and E at $t = 0.75, 1$.

# Chapter 5

# Concluding Remarks

In this thesis we studied the relationship between the optimal mapping used in the Monge-Kantorovich mass transfer problem and the idea of adaptivity used in moving mesh methods. We extend this study to consider the link between the idea of adaptivity of moving mesh methods and the transformation techniques found in the literature of fluid dynamics, the semi-geostrophic equations in meteorology, computational anatomy and image registration. We also showed that the mesh velocity field in the GCL method can be determined via a Monge-Kantorovich framework, and it is shown that the obtained velocity by this framework is a gradient of some potential function. This agrees with the results of the GCL method. It is shown that the solution of the Monge-Kantorovich mass transfer problem, image registration problem, and the problem of finding an adaptive mesh in moving mesh theory all reduce to solving the Monge-Ampere equation. However, in the case of two-dimensional space the Monge-Ampere equation derived in each of these problems is a highly non-linear second-order equation, and its numerical solution is very challenging. Some alternatives are required to avoid a direct use of a Monge-Ampere equation to solve those problems.

Further investigation is needed in order to be able to employ the transformation techniques that have been used in moving mesh methods for obtaining adaptive meshes, for solving the optimal mass transportation mapping problem, with the goal of obtaining better results than the other methods that have been used to solve MKP.

In the future we would like to develop the above mentioned relationships in such a way that enables us to use co-ordinate transformation techniques for moving mesh methods to solve some interesting problems in some fields of applied mathematics including fluid dynamics problems, the optimal mass transportation problem and the image registration problem.

# Bibliography


[1] W. Cao, W. Huang, and R. D. Russell, *A moving mesh method based on the geometric conservation law*, SIAM J. Sci. Comput., 24, pp. 118-142,2002.

[2] J. Benamou, Y. Brenier, *A computational fluid mechanics solution to the Monge-Kantorovich mass transfer problem*, Numer. Math., 84, pp. 375-393, 2000.

[3] Y. Brenier, *Polar factorization and monotone rearrangement of vector-valued functions*, Comm. Pure Appl. Math., 44, pp. 375-417, 1991.

[4] P. D. Thomas and Lombard, *Geometric conservation law and its application to the flow computations on moving grids*, AIAA J. 17, pp. 1030-1037, 1979.

[5] W. Huang, Y. Ren and R.D. Russell, *Moving mesh partial differential equations based on the equidistribution principle.* SIAM J. Numer. Anal. 31, no. 3, pp. 709-730, 1994.

[6] L. V. Kantorovich, *On a problem of Monge*, Uspekhi Mat. Nauk. 3, pp. 225-226, 1948.

[7] M. Knott, C. S. Smith, *On the optimal mapping of distributions*, J. Optim. Theory Appl. 43, no. 1, pp. 39-49.

[8] A. B. White, *On the numerical solution of initial/boundary-value problems in one space dimension*, SIAM J. Numer. Anal. 19 (1982), pp. 683-697.

[9] W. Huang, Y. Ren, R. D. Russell, *Moving mesh partial differential equations (MMPDEs) based on the equidistribution principle*, SIAM J. Numer. Anal., 31 (1994), pp. 709-730.

[10] K. Miller and R. N. Miller, *Moving finite elements I*, SIAM J. Numer. Anal., 18, 1019-1032, 1981.

[11] K. Miller, *Moving Finite Elements II*, SIAM J. Numer. Anal., 18, pp. 1033 - 1057, 1981.

[12] P. Bochev, G. Liao, and G. Pena, *Analysis and computation of adaptive moving grids by deformation*, Numer. Meth. PDEs, 12 (1996), pp. 489-506.

[13] Y. Ren and R. D. Russell, *Moving mesh techniques based upon equidistribution, and their stability*, SIAM J. Sci. Stat. Comput., 13, no. 6, pp. 1265-1286, Nov. 1992.

[14] C. de Boor, *Good approximation by splines with variable knots*. II, in Springer Lecture Notes Series 363, Springer-Verlag, berlin, 1973.

[15] D. S. Dodson, *Optimal order approximation by polynomial spline functions* Ph.D. thesis, Purdue University, West Layette, IN, 1972.

[16] J. M. Coyle, J. E. Flaherty, and R. Ludwig, *On the stability of mesh equidistribution strategies for time-dependent partial differential equations*, J. Comput. Phys., 62 (1986), pp. 26-39.

[17] C. J. Budd and J. F. Williams, *The parabolic Monge-Ampere equation in arbitrary dimension*, to appear.

[18] J. M. Hyman, *Adaptive moving mesh methods for partial differential equations*, in Advances in Reactor Computations, American Nuclear Society Press, La Grange Park, IL 1983, pp. 24-43.

[19] L. R. Petzold, *Observations on an adaptive moving grid method for one-dimensional systems of partial differential equations*, Appl. Numer. Math., 3, pp. 347-360, 1987.

[20] W. E. Schiesser, *Numerical Methods of Lines: Integration of Partial Differential Equations*, Academic Press, 1991.

[21] P.A. Zegeling and J. G. Blom, *An evaluation of the Gradient-Weighted Moving-Finite-Element Method in One Space Dimension*, J. Comput. Phys., Vol. 103, No. 1, p. 422, 1992.

[22] W. Huang and R. D. Russell, *A high dimensional moving mesh strategy*, Appl. Numer. Math., 26, pp. 998-1015, 1999.

[23] J. Chen, *Numerical Study of Blowup Problems and Conservation Laws with Moving Mesh Methods*, M. Sc. thesis, Simon Fraser University, Burnaby, B.C., Canada, 1991.

[24] M. I. Miller, A. Trouve, and L. Younes, *On the metric and Euler-Lagrange equations of computational anatomy*, Annu. Rev. Biomed. Eng., 4:375-405, 2002.

[25] M. F. Beg, M. I. Miller, A. Trouve, and L. Younes, *Computing metrics via geodesics on flows of diffeomorphisms*, preprint, Feb. 2003.

[26] A. Trouve, *Diffeomorphic groups and pattern matching in image analysis*, Int. J. Comp. Vision, 28, pp. 213-221, 1998.

[27] P. Dupuis, U. Grenander, and M. I. Miller, *Variational problems on flows of diffeomorphisms for image matching*, Quart. App. Math., LVI:pp. 587-600, Sep. 1998.

[28] S. Haker, A. Tannenbaum and R. Kikinis, *Mass preserving mapping and image registration*, in Proceedings of the Medical Image Computing and Computer-Assisted Intervention (MICCAI'01), 4th International Conference, Utrecht, The Netherlands, 2001.

[29] S. Haker, A. Tannenbaum and S. Angenent, *Optimal transport and image registration*, Internat. J. Comp. Vision, submitted.

[30] J. M. Fitzpatrick, *The existence of geometrical density-image transformations corresponding to object motion*, Computer Vision, Graphics and Image Processing, vol. 44, no. 2, pp. 155-174, 1988.

[31] S. Angenent, S. Haker and A. Tannenbaum, *Minimizing flows for the Monge-Kantorovich problem*, SIAM J. Math. Anal., 35, pp. 61-97, 2003.

[32] C. J. Budd and M. D. Piggott, *The geometric integration of scale-invariant ordinary and partial differential equations*, J. Comput. App. Math., 128, 399-422, 2001.

[33] C. J. Budd and M. D. Piggott, *Geometric integration and its applications*, Proceedings of ECMWF workshop on 'Developments in numerical methods for very high resolution global models', 93-118, 2000.

[34] M.J.P. Cullen and R. J. Douglas, *Applications of the Monge-Ampere equation and Monge transport problem to meteorology and oceanography* , Contemp. Math., 226, pp. 33-52, 1999.

[35] D. Mumford, *Pattern theory and vision*, In Questions Mathématiques En Traitement Du Signal et de L'Image, Capter 3, pp. 7-13. Paris: Institut Henri Poincaré, 1998.

[36] B.J. Hoskins, *The geostrophic momentum approximation and the semi-geostrophic equations.* J. Atmospheric Sci. 32, (1975) pp. 233-242.

[37] S. Chynoweth and M.J. Sewell, *Dual variables in semi-geostrophic theory*, Proc. Roy. Soc. London, Sect. A, 424 (1989), pp. 155-186.

[38] M.J.P. Cullen, J. Norbury and R.J. Purser,*Generalized Lagrangian solutions for atmospheric and oceanic flows*, SIAM J. App. Math. , 51, pp. 20-30, 1991.

[39] Patrick Knupp and Stanly Stienberg, *Fundamentals of Grid Generation*, CCRC. Press. 1994.

[40] R. E. Ewing and M. F. Wheeler, *Galerkin methods for miscible displacement problems in porous media*, SIAM J. Numer. Anal., 17(3), pp. 351-365, 1980.

[41] J. Douglas, *Finite difference methods for two-phase incompressible flow in porous media*, SIAM J. Numer. Anal., 20(4), pp. 564-574, 1983.

[42] R. Abraham , J. E. Marsden and T. Ratiu, *Manifolds, Tensor Analysis, and Applications*, Reading, MA, Addison-Wesley, 1983.

[43] L. Miroslav, *Vector Calculus*, Ontario, Addison-Wesley, 1997.

[44] R. B. McQuistan, *Scalar and Vector Fields: A Physical Interpretation*, New York, John Wiley and Sons, 1965.

[45] L. D. Landau and E. M. Lifshitz, *Fluid Mechanics 2nd ed*, Oxford, England ; New York, Pergamon Press, 1987.

[46] S. Iyanaga and Y. Kawada, *Monge-Ampere Equations*, §276 in Encyclopedic Dictionary of Mathematics. Cambridge, MA: MIT Press, pp. 879-880, 1980.

[47] D. Zwillinger, *Handbook of Differential Equations, 3rd ed.*, Boston, MA: Academic Press, 1997.

[48] Ch. E. Gutierrez, *The Monge-Ampere Equation and Related Topics*, Temple University, Philadelphia, USA, 2001.